NASA Contractor Report CR–189149

ULTRA HIGH BYPASS NACELLE AERODYNAMICS

INLET FLOW–THROUGH HIGH ANGLE OF ATTACK DISTORTION TEST

Michael J. Larkin and Paul S. Schweiger

Pratt & Whitney
Commercial Engine Business
East Hartford, CT 06108

July 1992

Prepared for:
NASA Lewis Research Center
Under Contract NAS3–25952

National Aeronautics and Space Administration

FOREWORD

This report presents the results of a study conducted to assess the impact of a fan or propulsor on subsonic transport nacelle inlet aerodynamics. This study was conducted as Task Order 8 under the Aero–Propulsion Technology (APT) program, NASA Contract NAS3–25952, under the direction of Mr. M. Bailey, NASA Program Manager.

The NASA Task Manager for Task 8 is Mr. Donald R. Boldman and Mr. Michael J. Larkin served as Task Manager for Pratt & Whitney. Acknowledgements are given to the following personnel for their technical support and contribution to the program: Paul S. Schweiger, coauthor and principal investigator; Thomas A. Wynosky, Wesley K. Lord, John E. McCall, Marlin W. DeVries and Christopher Ogden. Acknowledgement is also given to UTRC for their efforts in conducting the test.

Table of Contents

Table of Contents (Continued)

List of Tables

List of Figures

List of Figures (Continued)

1. SUMMARY

A flow–through inlet test program was conducted to evaluate inlet test methods and determine the impact of the fan on inlet separation when operating at large angles of attack. A total of 16 model configurations of approximately 1/6 scale (nacelle maximum diameter $\sim$ 20") were tested. The inlets and rake instrumentation were used in previous Advanced Ducted Prop 17" (fan diameter) powered rig tests. A comparison of these flow–through results with powered data indicates the presence of the fan increased separation free angle of attack operation 5° to 6° over the flow through inlet. When the instrumentation pole rakes are removed from the powered model's inlet diffuser, the 5° to 6° disparity is reduced to 3° to 4°. Rods and screens located at the fan face station, that redistribute the flow, achieved simulation of the powered–fan separation angle of attack (but did not duplicate the distortion patterns). Concepts to reduce inlet distortion and increase angle of attack capability were also evaluated. Vortex generators located on the inlet surface increased inlet angle of attack capability up to 2° and reduced inlet distortion in the separated region. Finally, a method of simulating the fan/inlet aerodynamic interaction using blockage sizing method has been defined. With this method, a static blockage device used with a flow–through model will approximate the same inlet onset of separation angle of attack and distortion pattern that would be obtained with an inlet model containing a powered fan.

2. INTRODUCTION

2.1 BACKGROUND

The historical method for determining inlet distortion and fan surge margin starts with testing flow–through inlet models to determine if the inlet is separated and/or generating total pressure distortion patterns when operated at high angles of attack or high crosswinds. These patterns are then simulated with screens that produce the same total pressure drop "smile" pattern observed in the flow–through test. The screens are installed in a fan rig (shown in Figure 1) where tests are conducted to verify sufficient fan surge margin and stability. Similar tests are also conducted with full scale engines.

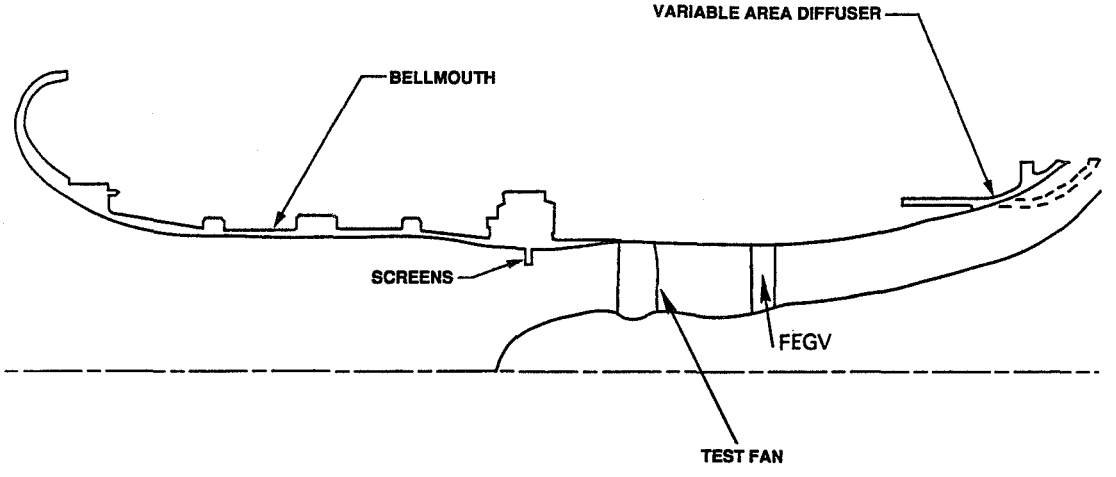

Figure 1 Fan Surge Margin/Stability Test Configuration

Recent ADP fan/inlet interaction rig tests conducted at NASA Lewis were compared to earlier flow–through/remote suction inlet test results. The comparison implied that the fan operation delays inlet distortion (see Figure 2). However, the inlet geometries and instrumentation were not identical (see Figure 3).

In addition, the absolute airflow for the fan rig was difficult to ascertain and set precisely. To acquire true back–to–back inlet aero data with and without a fan, the powered rig inlet hardware and instrumentation used for distortion testing at NASA was removed from the powered rig and mounted on a remote suction pipe at UTRC to repeat the distortion tests without a fan. Airflow was measured with a venturi for the flow–through test, thereby eliminating the airflow uncertainty of the powered rig test. The data from the flow through test was then compared to the Advanced Ducted Prop 17" Rig NASA tests results.

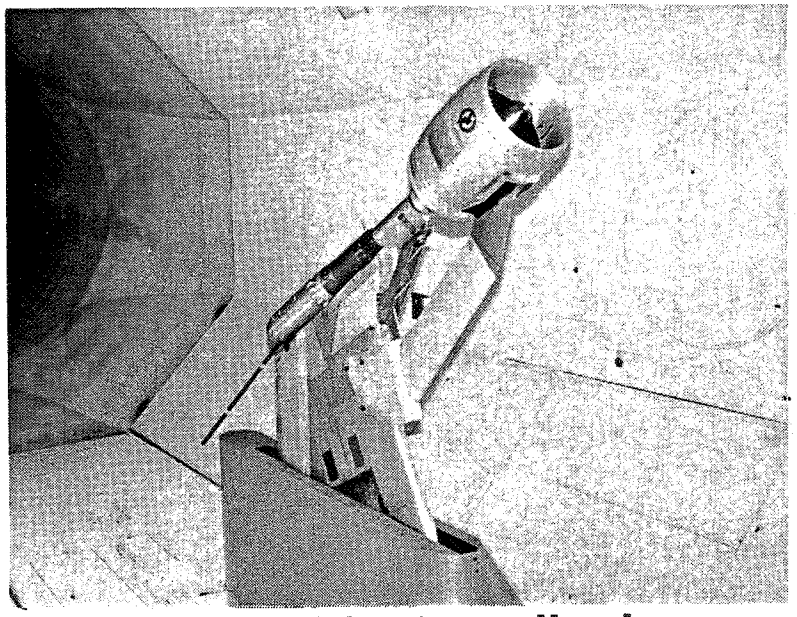

Powered fan/nacelle rig

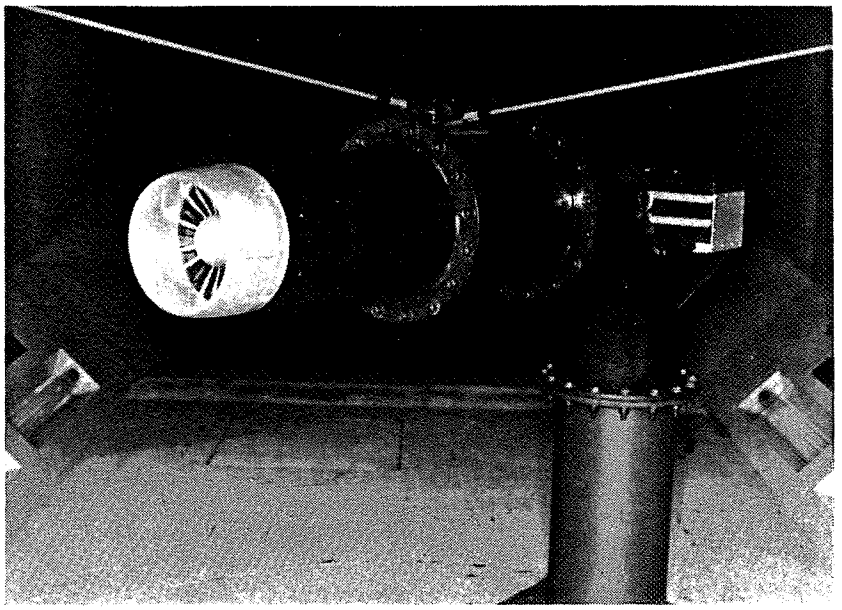

Flow-through/remote suction

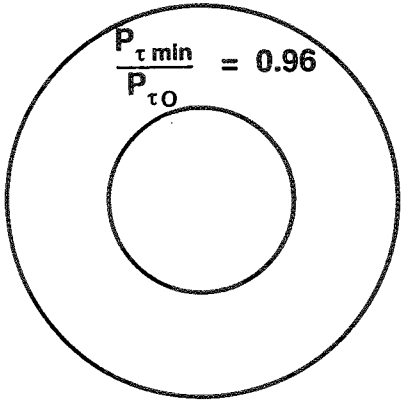

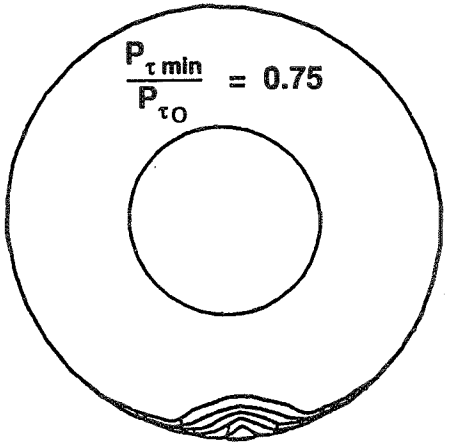

Figure 2 *ADP Fan/Inlet Interaction Rig Test Results Implied That the Fan Operation Delays Inlet Distortion*

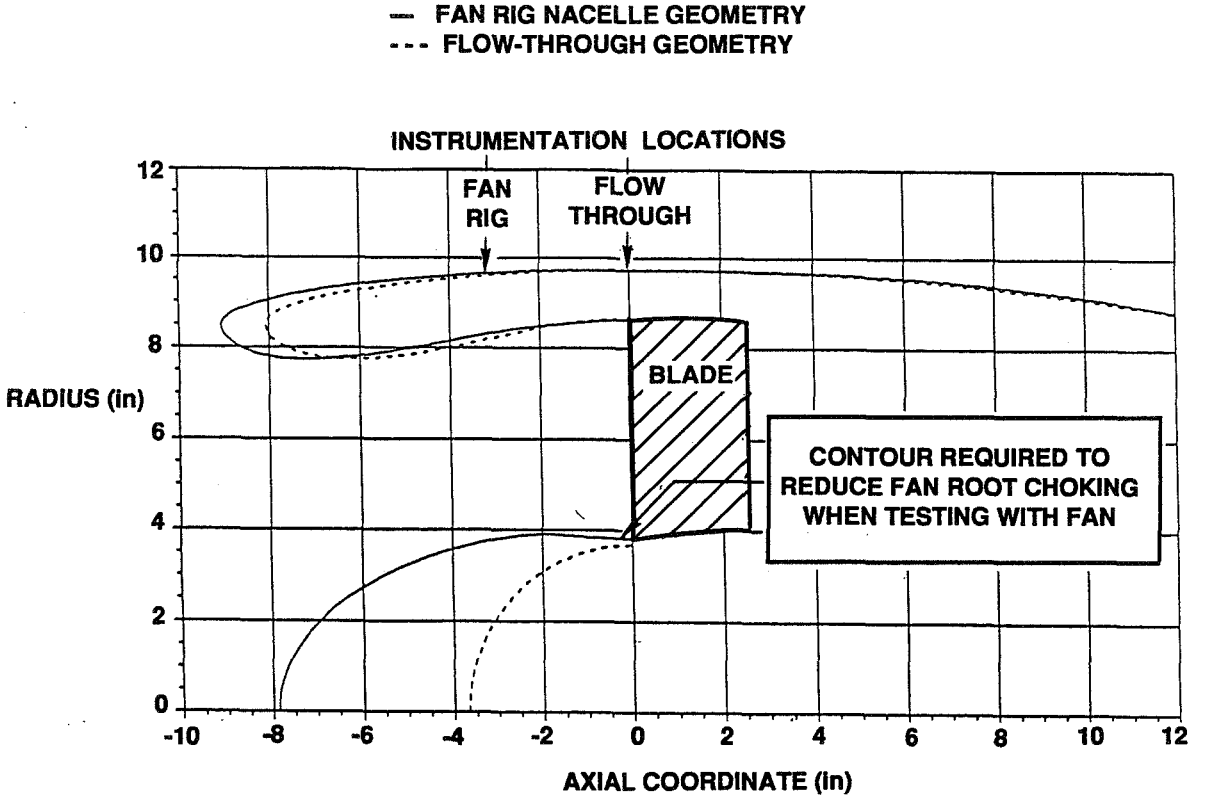

Figure 3 *Geometry Differencer*

2.2 OBJECTIVES

The primary program objective was to determine the impact of the fan presence on inlet separation angle of attack. A second objective was to formulate improved inlet flow through test methods and procedures to simulate the fan presence. The feasibility of simulating the fan with blockage such as rods, screens and combinations of rods and screens was to be assessed. A third objective was to obtain pressure data for CFD code verification. These included inlet surface static pressure at various axial and circumferential locations, and radial total pressure at two axial locations. The final objective was to test concepts, such as vortex generators, in an attempt to increase angle of attack capability and reduce inlet distortion.

3. MODEL AERODYNAMIC DESIGN

3.1 GEOMETRIC DEFINITION & DESIGN CRITERIA

3.1.1 Inlets

Figure 4 shows a comparison of the two inlet designs tested during the program and includes the significant geometric parameters for the two inlets. The baseline inlet was an aerodynamic design that utilized P&W standard design methods and had shapes suitable for low cruise drag, yet would not separate externally during windmill operation at 0.6 Mach number. The alternative inlet had an external plug with a centerbody extending forward of the inlet highlight plane. This feature allows shorting of the inlet cowl by unloading the cowl diffuser and taking internal diffusion in the centerbody.

CONFIGURATION	Dt	Dhl/Dt	Dhl/Dmax	Aff
BASELINE	15.480	1.0861	.8641	188.13
PLUG INLET	17.033	1.0828	.9178	188.13

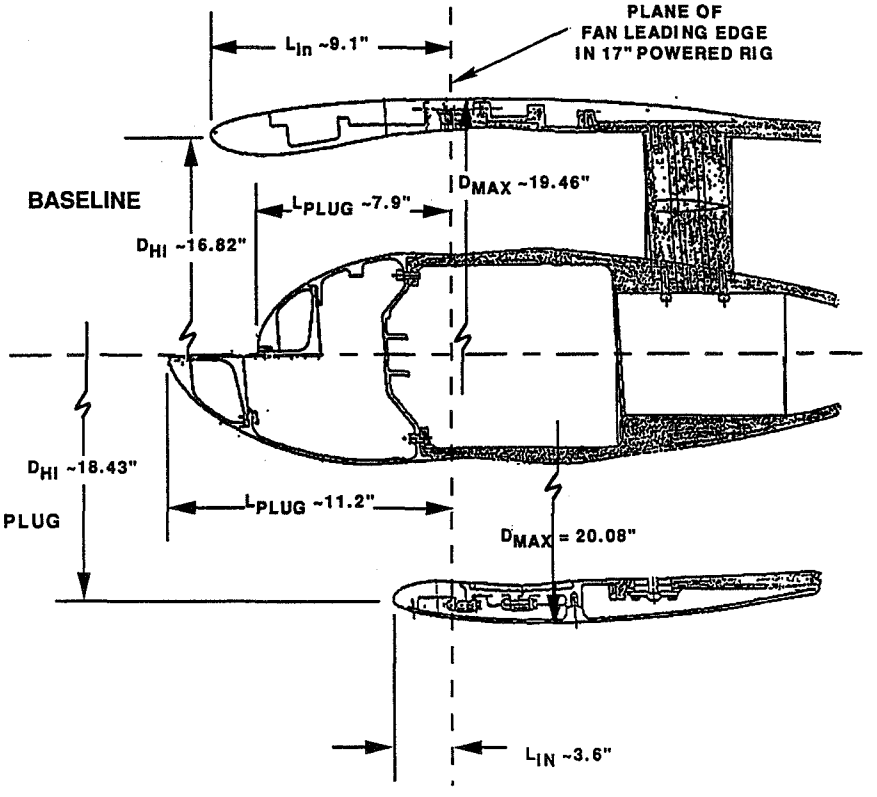

Figure 4 Two Inlets Were Tested

3.1.2 Fan Face Blockage

Different blockage arrays to simulate inlet/fan aero interaction were investigated. These included rods (including instrumentation rakes), screens and combinations of rods and screens. Flow redistribution to simulate the fan effect included openings at the inlet bottom, various percent blockage and various circumferential blockage patterns.

The investigations of the different fan face blockage schemes were done using the conventional inlet with the instrumentation located at the fan face station. Various blockage devices were used during the test to simulate the presence of the fan and its effect on inlet performance. Tapered blockage rods were installed at the fan face station. Uniform and nonuniform screens were installed just downstream of the fan face instrumentation. Finally, combinations of nonuniformly distributed blockage rods with overlaid screen patches were mounted at the fan face station.

Figures 5–8 define the fan face blockage schemes tested for each configuration. The blockage design approach included flow–through, which had insignificant blockage (3.0%) and consisted of the instrumentation only. The nominal blockage was 37% and was constant for most configurations. Blockage was varied on 5 configurations and different open area/blockage arrays were also tested to determine their effect on distortion hole size and depth. The design intent was to have choked flow at the maximum airflow through the blockage device. A summary of the blockage patterns is shown in Figure 9.

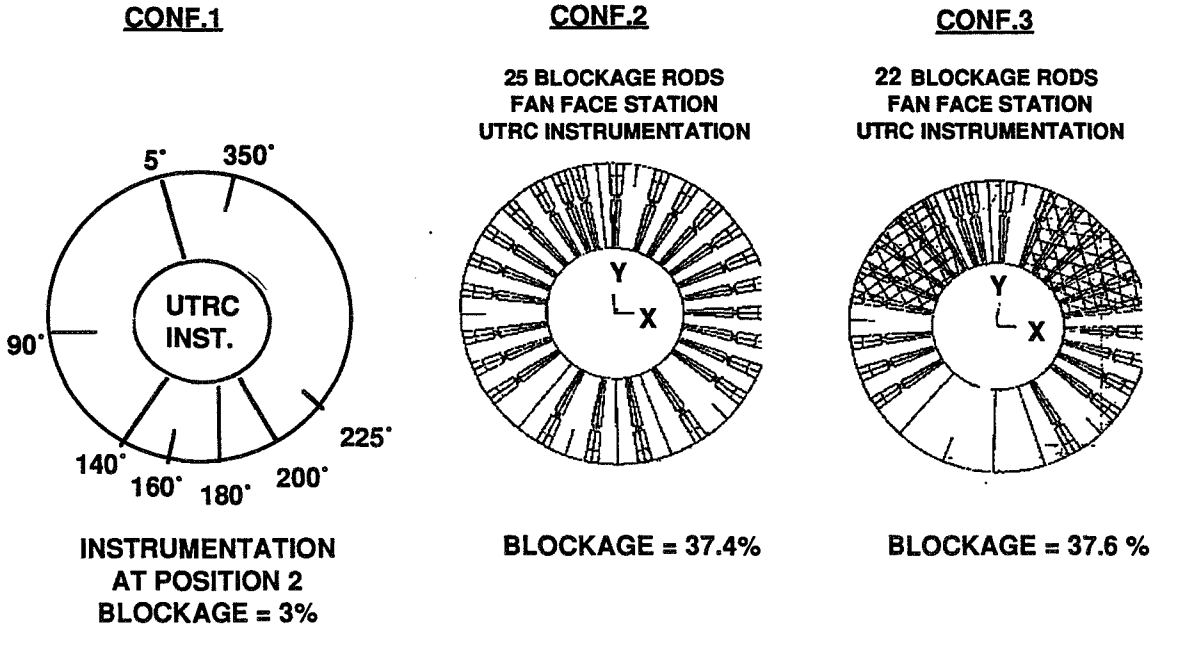

Figure 5 *Stationary Blockage Array Used With Baseline Inlet*

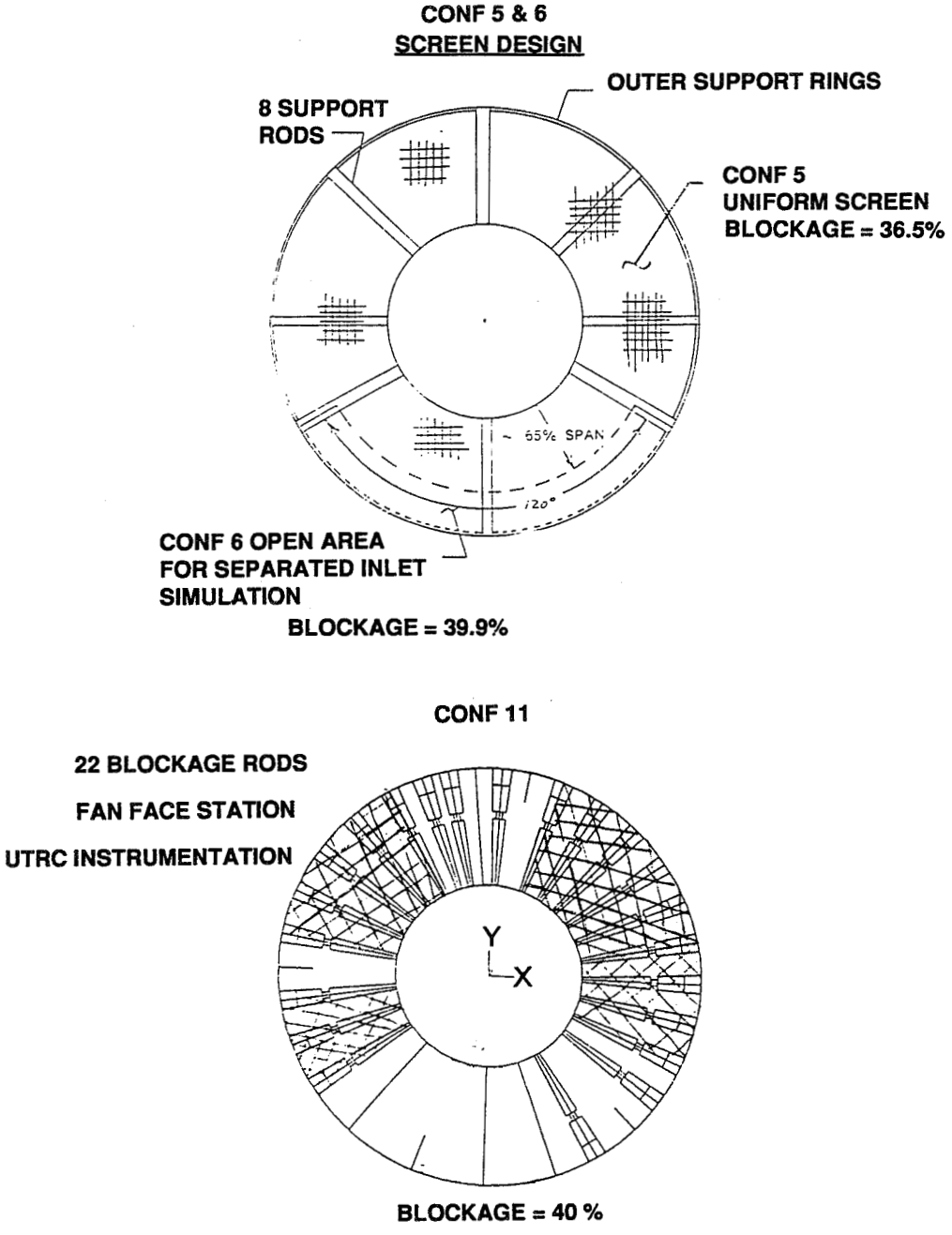

Figure 6 *Screen and Rod Patterns With the Baseline Inlet*

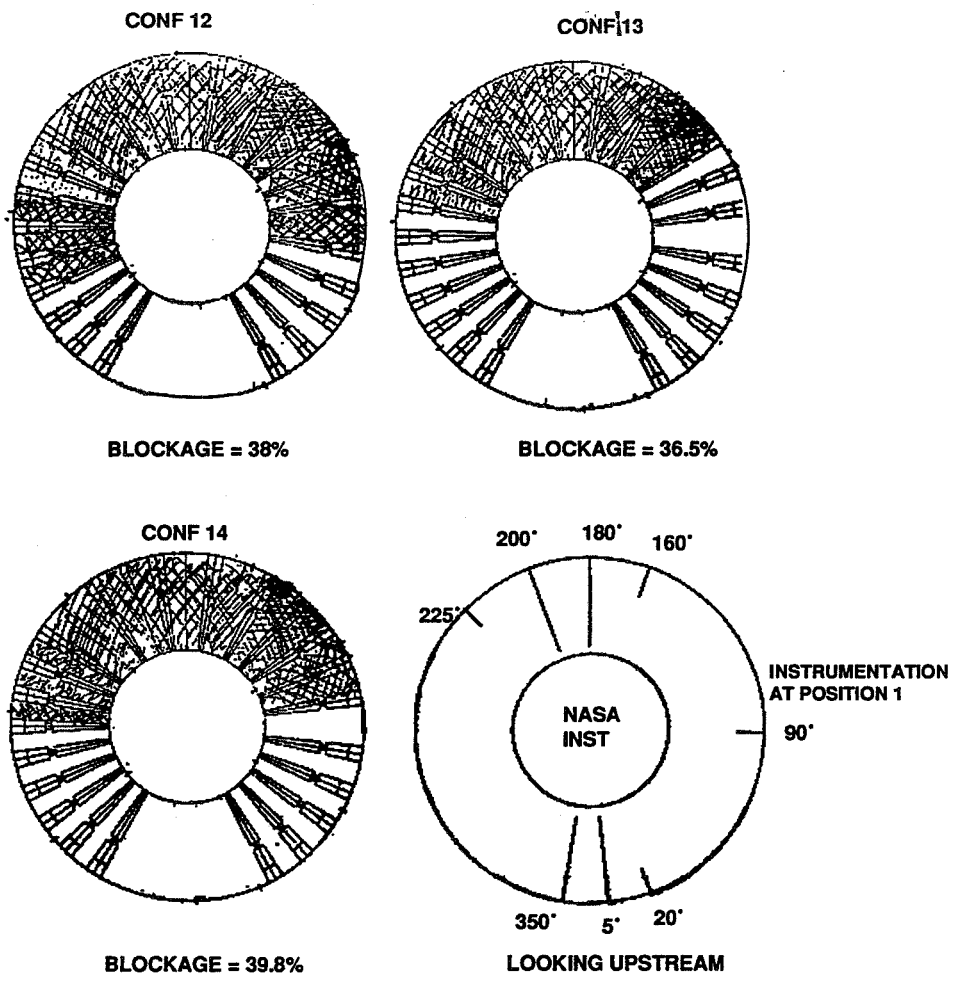

Figure 7 *Screen and Rod Patterns Used With the Baseline Inlet*

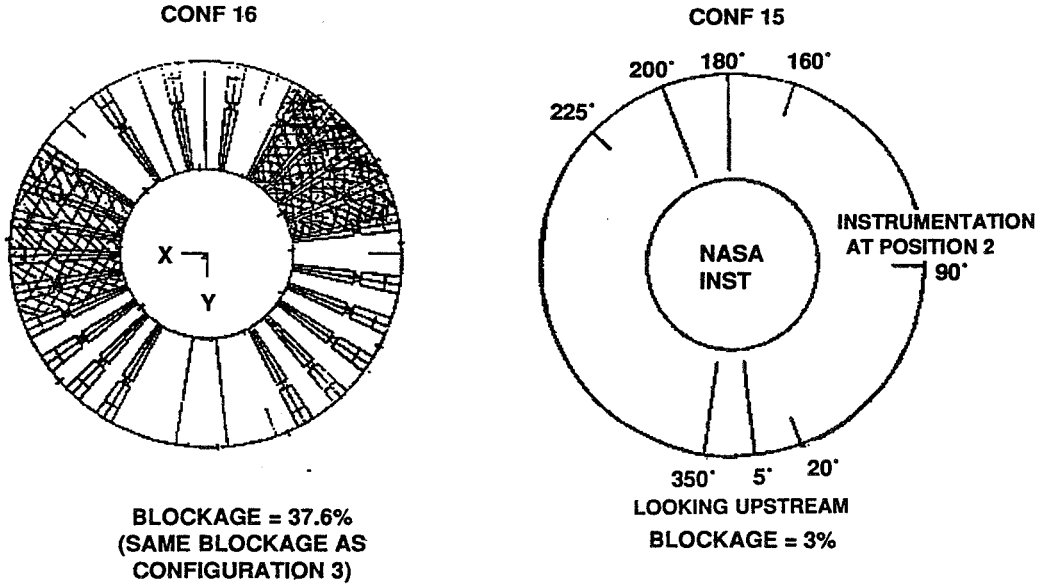

Figure 8 *Plug Inlet Blockage Patterns*

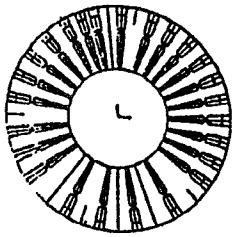

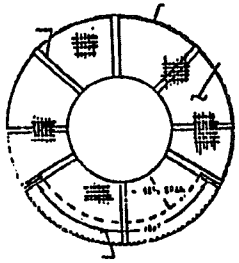

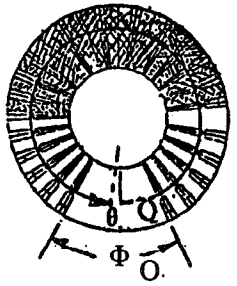

ϕ_R CIRCUMFERENTIAL COVERAGE OF RODS
ϕ_S CIRCUMFERENTIAL COVERAGE OF SCREENS
ϕ_O CIRCUMFERENTIAL COVERAGE OF OPEN AREA

θ_R LOCATION OF RODS BLOCKAGE CENTER
θ_S LOCATION OF SCREEN BLOCKAGE CENTER
θ_O LOCATION OF OPEN AREA CENTER

CONF.	Φ R	θ R	Φ S	θ S	Φ O	θ O	TRUE BLOCKAGE	COMMENTS
1	NONE		NONE		—		3.0%	INSTRUMENTATION ONLY
2	360	180	NONE		NONE		37.4%	25 RODS ONLY
3	273	169	A) 51	235	88	349	37.6%	22 RODS & SCREENS
			B) 59	131				
4	SAME AS CONF 3							TRIP STRIP
5	NONE		360	180	NONE		36.5%	UNIFORM SCREEN
6	NONE		240	180	120	0	39.9%	NON-UNIFORM SCREEN 65 – 100% OPEN
7, 8, 9, 10	SAME AS CONF 3							VORTEX GENERATOR TEST
11	273	169	A) 26	292	88	349	40.0%	22 RODS & SCREENS
			B) 51	235				
			C) 94	113				
12	276	193	170	185	84	13	38.0%	22 RODS & SCREENS
13	276	193	133	192	84	13	36.5%	22 RODS & SCREENS
14	276	193	213	187	84	13	39.8%	22 RODS & SCREENS
15	NONE		NONE		—		3.0%	INSTRUMENTATION ONLY
16	276	193	A) 59	264	84	13	37.6%	22 RODS & SCREENS
			51	125				

Figure 9 Blockage Patterns

The studies identified the fan face blockage scheme which provided the highest inlet separation angle of attack. This blockage (40% blockage, Configuration 11) pattern was then run with the instrumentation moved forward to position 1 to repeat the geometry run during the 9x15 ft. powered tests.

The use of blockage devices to simulate fan effects is dependent upon the flow capability of the vacuum system used. Adequate system flow capacity must be provided to supply the required flow despite the combined pressure loss of the model, piping and blockage devices. These techniques are most effective when the Mach number within the blockage device exceeds 0.8. Premature choking in the inlet or in the ducting downstream of the model could limit the effectiveness of the blockage devices to simulate the fan aero interaction.

3.1.2.1 Rod Design

The rods were designed to choke the inlet model fan face at the maximum air flow. A one–dimensional calculation was used to determine the critical fan face area less the blockage of the rods, screens and/or instrumentation poles. This area was corrected to account for an empirical flow coefficient (CD = 0.92) observed in previous testing.

The number of rods used is dependent on the location and amount of instrumentation. The rods should be placed away from static pressure instrumentation to avoid local flow field affects. An adequate number of rods should be used to give a circumferentially uniform blockage. The area of an individual rod is the total rod blockage area divided by the number of rods needed.

The rods were then sized to give the needed blockage area. A conical shape was used to give radially uniform flow area. The outer and inner rod diameters used should give equal circumferential blockage at the end walls. Some iteration is required to give the best combination of rod number and size to meet the blockage area.

3.1.2.2 Screen Design

Uniform and nonuniform screens were designed and installed just aft of the fan face instrumentation trailing edge. The screens were supported by eight evenly spaced cylindrical rods. Outer and inner support rings were installed to prevent screen bowing during testing.

The design intent was to have screens that choke at the same flow levels as the blockage rods. Difficulty in obtaining screen material did not allow exact flow matches. These flow anomalies are described in section 5.0.

The desired screen solidity is a function of the expected Mach number entering the screen. The entering one–dimensional Mach number was calculated using the air flow and

available flow area. The flow area was the remaining duct area after adjustment for screen support hardware and instrumentation blockage. Data from available publications (references 1 & 2) were used to determine the screen solidity. A screen material with adequate wire diameter (0.047 to 0.063 inch) was selected to ensure screen structural integrity.

The open area in the nonuniform screen was sized to provide approximately the same increase in open area as removing three of the blockage rods. The solidity of the remaining screen was increased in an attempt to keep the fan face blockage consistent with the uniform screen.

3.1.2.3 Screen and Blockage Rod Combinations

An alternative simulation of the fan under separated conditions was accomplished by opening a hole in the fan face blockage in the region where flow separation had been observed during the powered rig tests. The displaced blockage was moved to the opposite side of the fan face in an attempt to drive the flow toward the hole to delay the onset of the inlet separation. Previous testing has shown that the circumferential extent of the distorted region, at the fan face at separation, is approximately 90 degrees. An opening in the fan face blockage of approximately this size was made by removing three blockage rods. The blockage of the three rods was compensated for by laying screen patches directly over the remaining rods away from the total pressure instrumentation.

The size of the screen patches was dependent on the blockage needed and the solidity of the screen. The screen provided blockage by covering the open spaces between the rods. The size of the required patch was determined by assuming a patch size and calculating the available open flow area over the region. The blockage provided by the screen covering this open area was then compared to the blockage of the removed rods. Some iteration was necessary to achieve the correct patch size. The patches were split into sections to avoid covering the total pressure instrumentation and were always ended at a rod location to avoid exposing an unsupported edge to the flow.

4. TEST FACILITY AND TEST PROGRAM

4.1 TEST FACILITY

The test facility used in this program was the 10x15 ft. test section of the United Technologies Research Center Large Subsonic Wind Tunnel (LSWT). Figure 10 shows the model installed in the test section. The test section is capable of speeds up to Mach 0.38. The tunnel operates at atmospheric stagnation pressure with the stagnation temperature held between 60 and 140°F and is equipped with a remote suction system giving a maximum flow of 44.6 lbs/sec corrected flow. Vacuum is provided by an Allis–Chalmers compressor driven by a gas turbine remotely located from the tunnel. A pipe line connects the vacuum source to the tunnel facility. Figure 11 shows a schematic of the test facility with the suction system piping in place. The inlet model was mounted directly to the system piping through the use of an adapter. A leak check of the system was performed with the inlet removed by capping the adapter flange and applying vacuum downstream.

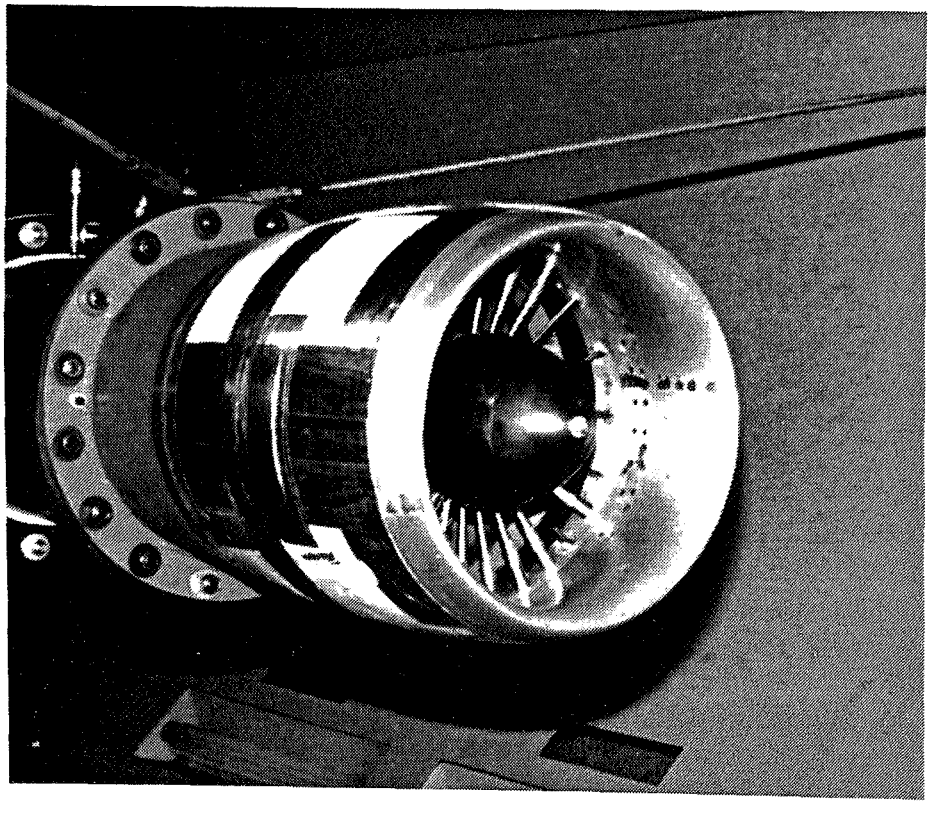

Figure 10 PW/ADP Aspirated Inlet Test Setup

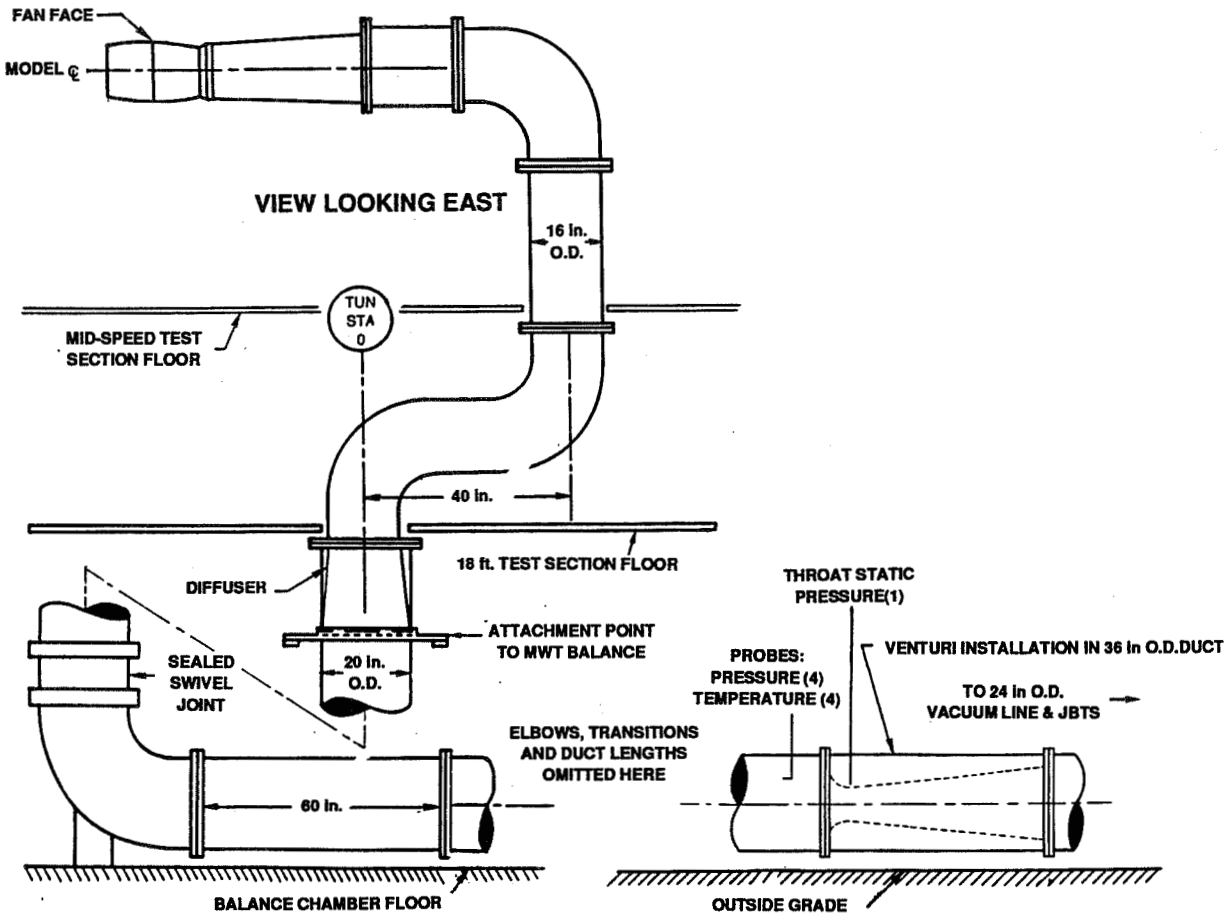

Figure 11 General Model Installation Schematic

The inlet model centerline was located near the tunnel centerline. The model was rolled 90 degrees so that inlet pitching could be simulated by yawing the model assembly about a horizontal plane. The vacuum piping passing through the tunnel floor turntable was fitted with a sealed swivel joint that allowed the piping to rotate with the turntable when moved by remove control. The inlet model could be yawed to simulate a maximum angle of attack of 45 degrees.

Weight flow measurements during the test were made with a 18.9 in. diameter Bif Corporation venturi installed within the 36 in. diameter section of system piping. Four total pressure and four total temperature measurements along with one venturi throat static pressure measurement were used to calculate the ideal flow passing through the venturi. A flow coefficient calibration (Figure 12) based on the ratio of the venturi total pressure to throat static was used to determine the actual corrected flow passing through the venturi and inlet model.

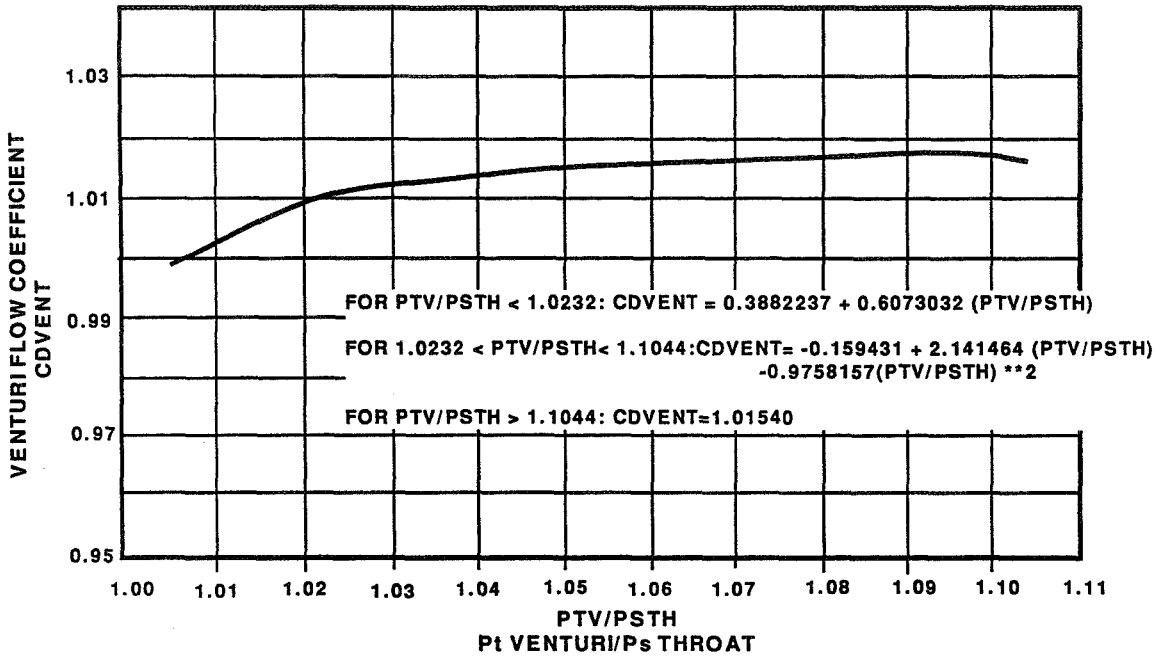

Figure 12 ADP/NASA UTRC Venturi Calibration Curves (June 1991)

All pressure measurements were made with scanivalves and all temperatures were determined with an ITI temperature scanner. All data was transmitted to Pratt and Whitney via direct data link and stored. The reduced data was then transmitted to NASA LeRC via data link.

4.2 TEST INSTRUMENTATION

The test instrumentation consisted of 8 total pressure rakes which could be located in either of two axial positions in the inlet model and surface static pressures located in axial and circumferential rows on the inlet model. Total pressures consisted of four pole rakes with 12 probes each and four boundary layer rakes with 9 probes each. Figure 13 shows the circumferential locations of the total pressure rakes at position 1 (located within the inlet diffuser) and position 2 (at the model fan face). Surface static pressure instrumentation consisted of 6 axial rows installed on the conventional inlet and 2 axial rows for the plug inlet (0 and 341 degrees). Each inlet model had 3 circumferential rings of static pressure taps, one in the inlet diffuser and two at the fan face.

A mass averaged and area averaged total pressure were calculated when the total pressure rakes were located at position 2 (fan face). An area averaged total pressure was calculated then the rakes were located at position 1 (inlet diffuser). The axial static pressures were normalized by free stream total pressure and converted to pressure coefficient form. The ring static pressures were normalized by free stream total pressure.

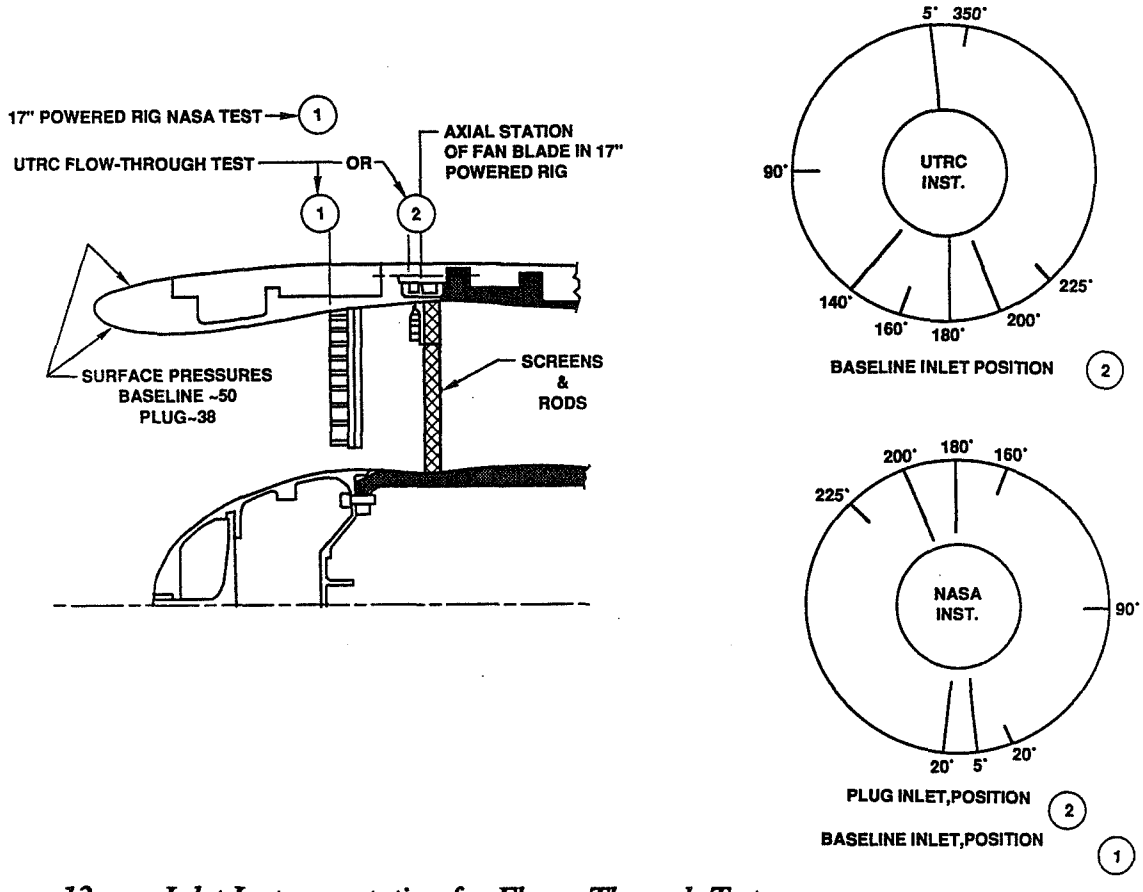

Figure 13 Inlet Instrumentation for Flow–Through Test

4.3 TEST PROGRAM

The test program consisted of test procedures, conditions, data acquisition and data reduction. The test conditions were set to repeat the conditions from the 9x15 ft. Powered Test run at NASA LeRC in 1990. The data reduction describes the total pressure averaging calculations, pressure normalization, distortion parameter and flow calculations.

4.3.1 Test Procedures

Two types of runs were performed to acquire the desired performance data:

1) Angle of attack variation at constant Mach number and corrected inlet weight flow.

2) Corrected weight flow variation at zero inlet angle of attack and constant tunnel Mach number.

For the angle variation runs, the desired test section Mach number and inlet corrected flow were established at zero inlet angle of attack. The weight flow level was held constant as

the inlet was pitched by making minor flow adjustments. The inlet was pitched upward in coarse increments of 2 degrees with data acquisition occurring at each step. Prior to the expected angle of separation, the steps were reduced to 1 degree. Data was acquired at 1 degree increments through separation to 3–5 degrees beyond the separation angle. The model was then returned to zero angle of attack and the next test condition was set.

The inlet separation angle was determined by monitoring the static and total pressure instrumentation on the model. Figure 14 shows how the instrumentation was used. The first figure shows that before the onset of inlet–separation, at a given angle of attack, the high rate of flow curvature around the inlet lip produces minimum pressure measurements which result in peak values of surface Mach numbers. As inlet angle of attack is increased, lip separation begins to occur producing a local separation bubble. This separation bubble causes a reduced rate of curvature and results in lower levels of peak Mach numbers. As the angle of attack is increased, the separation region grows until there is very little or no lip suction. In addition, the inlet separation produces a total pressure deficit in the separated region. The second figure shows the distortion parameter which is a measure of the total pressure loss. It should be noted that the surface pressures around the lip provide a reliable indication of inlet separation and was used as the primary indicator of separation.

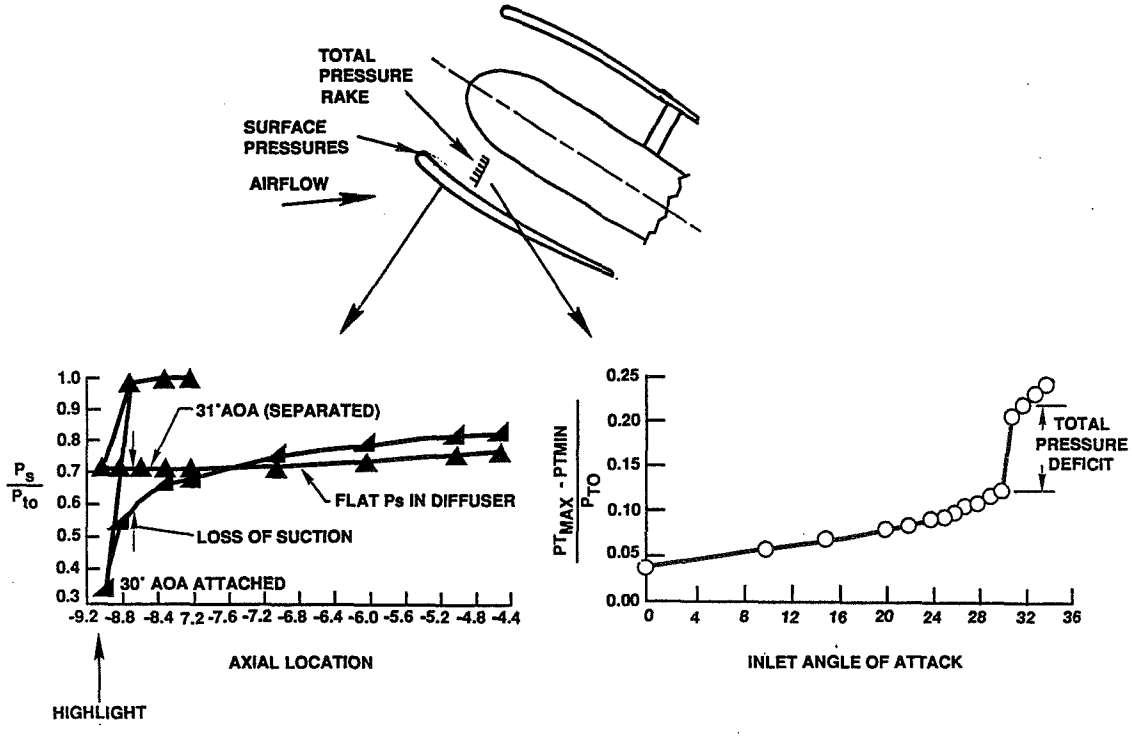

Figure 14 *Typical Changes In Pressure When Separation Occurs. Configuration 12, Mn = 0.2 Wc ~ 38.2 lbs/sec*

During the weight flow variation runs, the inlet angle of attack was held at zero degree and the test section Mach number was held constant. The weight flow passing through the model was increased in increments with data acquisition occurring at each step. Weight flow variations were controlled by valves located in the vacuum system piping or adjustment of the power setting on the vacuum source.

4.3.2 Test Conditions

The test run schedule is shown in Table I. The test was primarily run at Mach 0.20 to coincide with the data from the 9x15 NASA LeRC test. Flow levels were set in an attempt to repeat the powered model data as closely as possible. Inlet flow rates are typically expressed as flow per unit fan face area and these values are also shown in Table 1.

4.3.3 Data Acquisition and Reduction

The data reduction process begins with the reading of all the pressures and temperatures on the model and flow venturi. The venturi entrance conditions are determined by arithmetically averaging the venturi entrance total pressures and temperatures. The ideal venturi flow was calculated using the venturi throat area, the ratio of venturi total to throat static pressure ratio and entrance conditions. The actual flow was obtained by multiplying the ideal venturi flow with the venturi flow coefficient. The flow coefficient was obtained from a calibration based on venturi total to throat static pressure ratio. The flow was then corrected to standard day conditions.

Corrected flow was also calculated using an analytically derived flow calibration for the circumferential ring of static pressures at position 1. The calibration is based on the ratio of free stream total pressure to the arithmetic average of the 10 static pressures in the ring.

All model pressures are normalized by free stream total pressure. The axial rows of static pressures are converted to pressure coefficient form. The inlet angle of attack is also recorded.

The area averaged total pressure is calculated by multiplying each total pressure by the appropriate area factor and summing the products. At position 1, the ring of static pressures on the outer wall was also included in the area averaged total pressure by assigning area factors to those static pressures. The area averaged total pressure at position 2 does not include the wall static pressures. This same approach was used in the 17" powered fan where the inner wall static pressure was not measured since the centerbody was rotating. As a result, direct comparison of area average pressures can be made between the flow–through and powered rig results.

TABLE I. – TEST CONDITIONS

M_N = 0.20 TO 0.25

W_C = 29.3 TO 44.6 lb/sec

W_C/Aff = 22.43 to 33.68 lb/sec -ft^2

ANGLE OF ATTACK = 0° TO 46°

Run Schedule

Run	Conf.	Inlet	Mach	Alpha	Instrum. Location	WC (lb/sec)	Blockage	Remarks
12	1	Baseline	0.00	0	FF-UTRC	Vary	None	Shakedown
13	1	Baseline	0.20	0	FF-UTRC	0.0	None	Shakedown
14	1	Baseline	0.20	0	FF-UTRC	Vary	None	
15	1	Baseline	0.20	0/30	FF-UTRC	30.0	None	
16	1	Baseline	0.20	0/30	FF-UTRC	32.0	None	
17	1	Baseline	0.20	0/28	FF-UTRC	44.0	None	Maximum Flow
18	1	Baseline	0.20	0/29	FF-UTRC	38.0	None	
19	1	Baseline	0.20	0/29	FF-UTRC	40.0	None	
20	2	Baseline	0.20	0/29	FF-UTRC	39.7	25 Rods	Over Ranged X-Ducer
21	2	Baseline	0.20	0/29	FF-UTRC	39.5	25 Rods	
22	2	Baseline	0.25	0/29	FF-UTRC	39.3	25 Rods	
23	2	Baseline	0.25	0/32	FF-UTRC	30.0	25 Rods	
24	2	Baseline	0.20	0/32	FF-UTRC	31.5	25 Rods	
25	3	Baseline	0.00	0/21	FF-UTRC	39.6	Screen/Rod	
26	3	Baseline	0.20	0/30	FF-UTRC	26.0	Screen/Rod	
27	3	Baseline	0.20	0/32	FF-UTRC	31.5	Screen/Rod	
28	3	Baseline	0.20	0/29	FF-UTRC	38.2	Screen/Rod	Hysteresis Check
29	3	Baseline	0.20	0/33	FF-UTRC	30.0	Screen/Rod	
30	2	Baseline	0.20	0/33	FF-UTRC	29.3	25 Rods	
31	2	Baseline	0.20	0/31	FF-UTRC	38.2	25 Rods	
32	1	Baseline	0.20	0/26	FF-UTRC	44.0	None	Repeat of 17
33	1	Baseline	0.20	0/29	FF-UTRC	38.2	None	Repeat of 18
34	1	Baseline	0.20	0/28	FF-UTRC	40.0	None	Repeat of 19
35	1	Baseline	0.20	0/33	FF-UTRC	31.5	None	Repeat of 16
36	4	Baseline	0.20	0/32	FF-UTRC	39.7	Screen/Rod	Trip Strip
37	5	Baseline	0.20	0/33	FF-UTRC	39.5	Full Screen	
38	5	Baseline	0.20	0/32	FF-UTRC	38.2	Full Screen	
39	6	Baseline	0.20	0/33	FF-UTRC	39.4	Smile Screen	
40	6	Baseline	0.20	0/33	FF-UTRC	38.2	Smile Screen	
41	7	Baseline	0.20	0/32	FF-UTRC	39.5	Screen/Rod	Triangular VG

Run Schedule

Run	Conf.	Inlet	Mach	Alpha	Instrum. Location	WC (lb/sec)	Blockage	Remarks
42	7	Baseline	0.25	0/33	FF-UTRC	39.5	Screen/Rod	Triangular VG
43	8	Baseline	0.20	0/25	FF-UTRC	39.5	Screen/Rod	Bad Instrum.
44	8	Baseline	0.20	0/32	FF-UTRC	39.5	Screen/Rod	Triangular VG
45	9	Baseline	0.20	0/32	FF-UTRC	39.5	Screen/Rod	Candle Flame VG
46	10	Baseline	0.20	0/33	FF-UTRC	39.5	Screen/Rod	Candle Flame VG
47	11	Baseline	0.20	0/33	FF-UTRC	38.0	Screen/Rod	More Blockage
48	12	Baseline	0.20	0/21	Inl-NASA	39.5	Screen/Rod	
49	12	Baseline	0.20	0/33	Inl-NASA	39.5	Screen/Rod	
50	12	Baseline	0.20	0/34	Inl-NASA	38.2	Screen/Rod	
51	12	Baseline	0.20	0/35	Inl-NASA	31.5	Screen/Rod	
52	13	Baseline	0.20	0/30	Inl-NASA	39.4	Screen/Rod	Less Blockage
53	13	Baseline	0.20	0/32	Inl-NASA	39.0	Screen/Rod	Less Blockage
54	14	Baseline	0.20	0/28	Inl-NASA	39.0	Screen/Rod	More Blockage
55	14	Baseline	0.20	0/31	Inl-NASA	38.2	Screen/Rod	More Blockage
56	14	Baseline	0.20	0/35	Inl-NASA	30.0	Screen/Rod	More Blockage
57	14	Baseline	0.20	0/35	Inl-NASA	31.5	Screen/Rod	More Blockage
58	15	Plug	0.20	0/40	FF-NASA	44.6	None	Shakedown
59	15	Plug	0.20	0/40	FF-NASA	39.5	None	
60	15	Plug	0.20	0/40	FF-NASA	38.2	None	
61	15	Plug	0.20	0/35	FF-NASA	44.6	None	Repeat of 58
62	15	Plug	0.20	0/36	FF-NASA	39.5	None	Repeat of 59
63	15	Plug	0.20	25/38	FF-NASA	38.2	None	Repeat of 60
64	15	Plug	0.20	0/42	FF-NASA	35.0	None	
65	16	Plug	0.20	0/46	FF-NASA	40.1	Rod/Screen	
66	16	Plug	0.20	0/45	FF-NASA	38.2	Rod/Screen	
67	16	Plug	0.20	0/45	FF-NASA	35.0	Rod/Screen	
68	16	Plug	0.20	30/43	FF-NASA	39.5	Rod/Screen	
69	16	Plug	0.20	30/43	FF-NASA	38.2	Rod/Screen	

The mass averaged total pressure was calculated only when the total pressure rakes were located at the fan face. Each total pressure probe was weighted by the portion of ideal flow passing through the area assigned to that probe. The static pressure for each rake was assumed to vary in a linear fashion between the inner and outer static pressure assigned each rake. Based on the probe radius, a static pressure was assigned to each probe on the rake. The total pressure probes closest to the outer wall were averaged with the local wall static pressure to account for the boundary layer. The probe total to static pressure ratio and area factor were then used to calculate a local ideal flow for each probe. Each total pressure reading was weighted by the ratio of the local ideal flow to the summation of the ideal flows for all the probes.

The distortion parameters were calculated as the difference between the highest and lowest total pressure measured divided by a representative average total pressure. The representative total pressure was either the free stream, mass averaged or area averaged total pressure calculated.

A complete listing of data reduction equations and instrumentation locations can be found in Appendix A.

5. TEST RESULTS AND ANALYSIS

The test data was transmitted to NASA LeRC via a data link at the completion of the test program. This section highlights the significant findings from analysis of these data.

5.1 BASELINE INLET

Various blockage patterns were tested in an attempt to simulate the 17" powered rig angle of attack where separation was first detected and to replicate the circumferential extent of the distortion "smile" and the deficit depth. Angle of attack, flight speed and inlet airflow were the principle variables. Limited plug inlet tests were conducted with the best fan simulation blockage pattern and will be discussed in section 5.2.

5.1.1 Flow–Through Tests

The first series of tests were conducted without rods and/or screen blockage, but with inlet total pressure instrumentation positioned at the axial station of the fan blade leading edge (position 2 of Figure 13) (Note that zero blockage was not achieved in that the presence of the instrumentation pole axis constitutes 3% flow blockage). Comparison of this flow–through data to the 17" rig results indicates that higher flow–through testing produces a pessimistic result. The presence of the fan allows the inlet to operate at separation–free angles of attack 5 degrees higher than the flow–through results would indicate (see Figure 15). It should be noted that the 17" rig results had distortion rakes in the inlet which subsequent diagnostic testing indicated reduces this 5° difference by 1° to 2°. This data is shown as a 1 degree band. The test procedure increased angle of attack in 1 degree increments until separation occurs. Typically, the lower value shown indicates the last angle of attached flow and the upper level is the point of full separation.

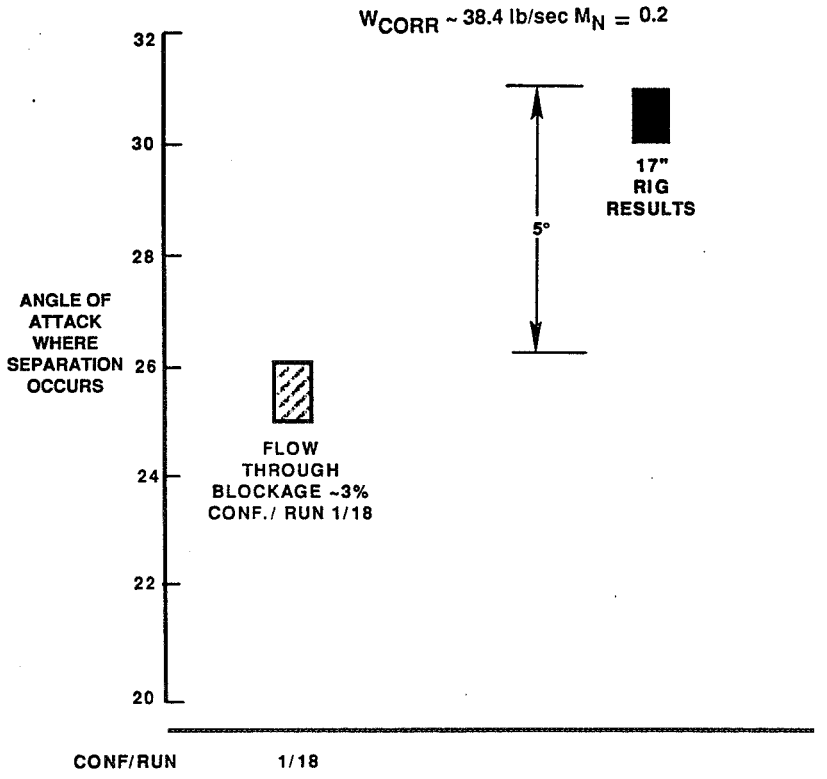

Figure 15 Presence of Fan Delayed Separation Angle of Attack 5° Over Flow Through Inlet

Rods and screens that redistribute the flow were effective in delaying the onset of separation. The variations of onset of separation angle of attack with blockage is shown in Figure 16. As blockage is increased with screens, rods or combination of rods and screens, the one dimensional Mach number through the blockage also increased for a given airflow. For 38.4 lbs/sec, the separation angle of attack appears to level off when the Mach number exceeded 0.8. Note that in this region the blockage devices closed to within 2 degrees of the 17" rig data.

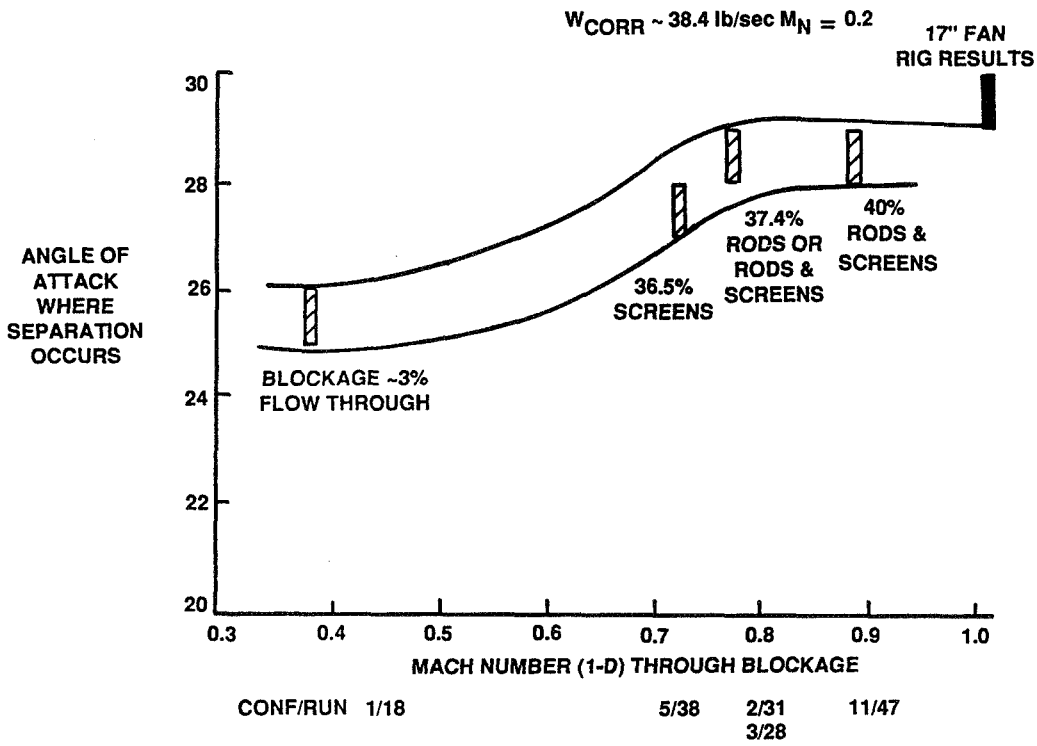

Figure 16 *Rods and Screens That Distribute Flow Achieved Fan Simulation to Within 1°. No Inlet Distortion Rakes.*

Increasing the inlet airflow had no impact on the flow–through inlet's angle of attack capability (Figure 17). This is contrary to engineering judgement. The higher airflows results in higher peak Mach numbers and stronger shocks at the inlet lip. Intuition would say it should separate sooner and when blockage was introduced, separation occurred (Figure 19). Note there's an apparent sensitivity to the type of blockage. Rods alone and screens alone differ from the rod and screen combination. Which one is the best simulation cannot be ascertained because the rig did not operate at this higher airflow.

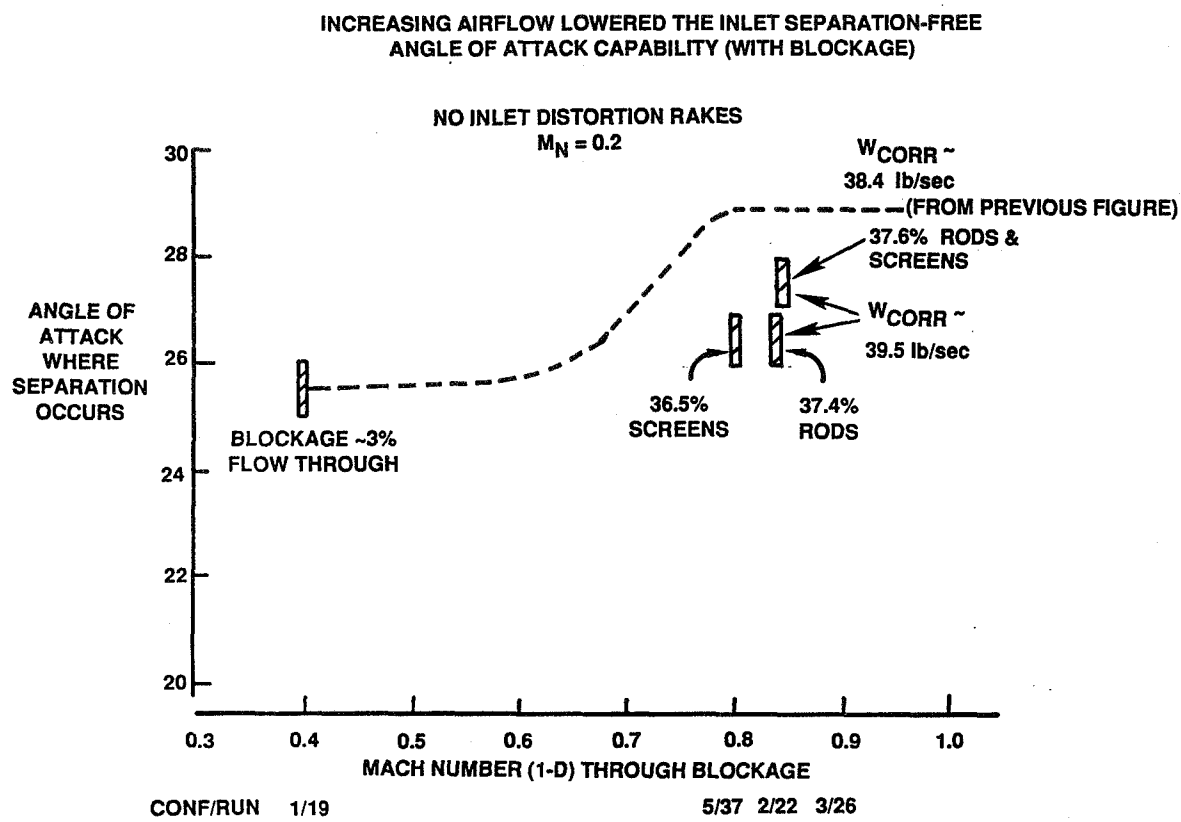

Figure 17 *Increasing Airflow Lowered the Inlet Separation – Free Angle of Attack Capability (with blockage).*

5.1.2 Distortion Rakes In Inlet

The second series of tests were conducted with the total pressure rakes located in the inlet diffuser at the same location in the 17" rig (position 1 in Figure 13). Figure 18 shows that the inlet distortion rakes increase separation free operation 2 degrees over test results without inlet instrumentation, and it now shows excellent agreement with the 17" rig results. It appears that blockage can be used to produce the same result as testing with a fan. Furthermore, the presence of the rakes in the diffuser reduces the diffuser area ratio and as a result, reduces the adverse pressure gradients which appears to be delaying the separation angle of attack. Testing with this instrumentation in place gives an overly optimistic result regarding when separation would occur. The best test technique would be to test for the onset of separation without this instrumentation and rely on wall static pressures for determining when separation occurs.

After separation occurs, attention shifts to how well the blockage devices simulated the total pressure distortion pattern in the separated region. The inlet diffuser (position 1) pole rake data was used to generate distortion patterns for the 17" rig and flow–through plus blockage test models. These are compared in Figure 19. At first glance they appear quite similar. Both are classical "smile" patterns of similar shape, radial penetration, and circumferential extent. However, the total pressure hole is 5 percent deeper than the rig data with PT minimum being 0.80 as compared to 0.85 with the 17" rig. The discrepancy was confirmed at two PT rake circumferentially located +5 degree and −10 degrees from bottom dead center (Figure 20).

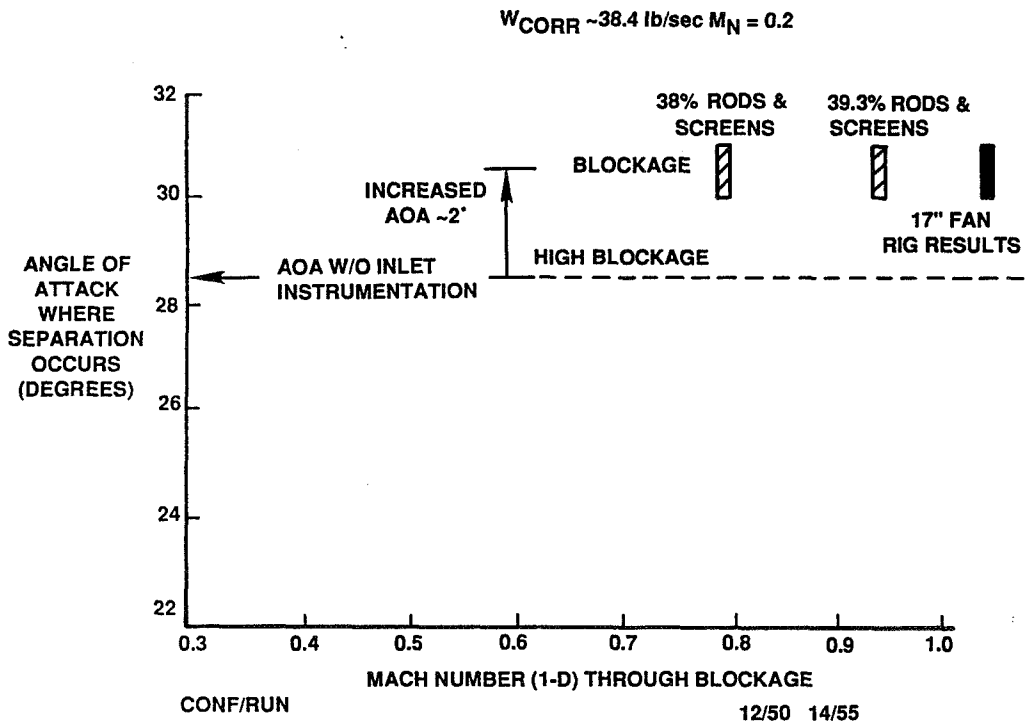

Figure 18 *Inlet Distortion Rakes In Inlet Diffuser Reduce Adverse Pressure Gradients and Increase Separation Free Operation 2°. Distortion Rakes In Inlet.*

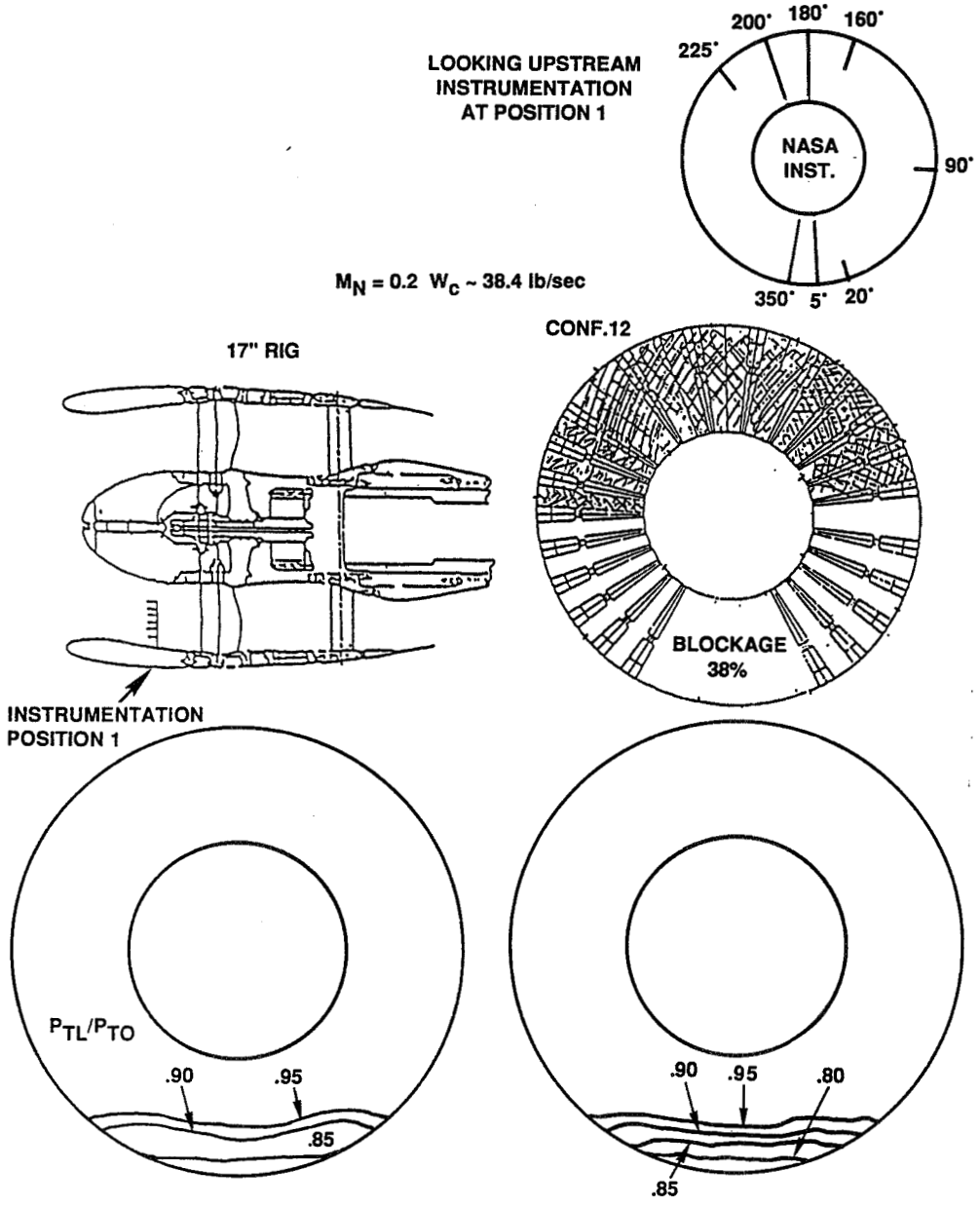

Figure 19 *Distortion Maps Are Similar In Width. Angle of Attack ~ 31°.*

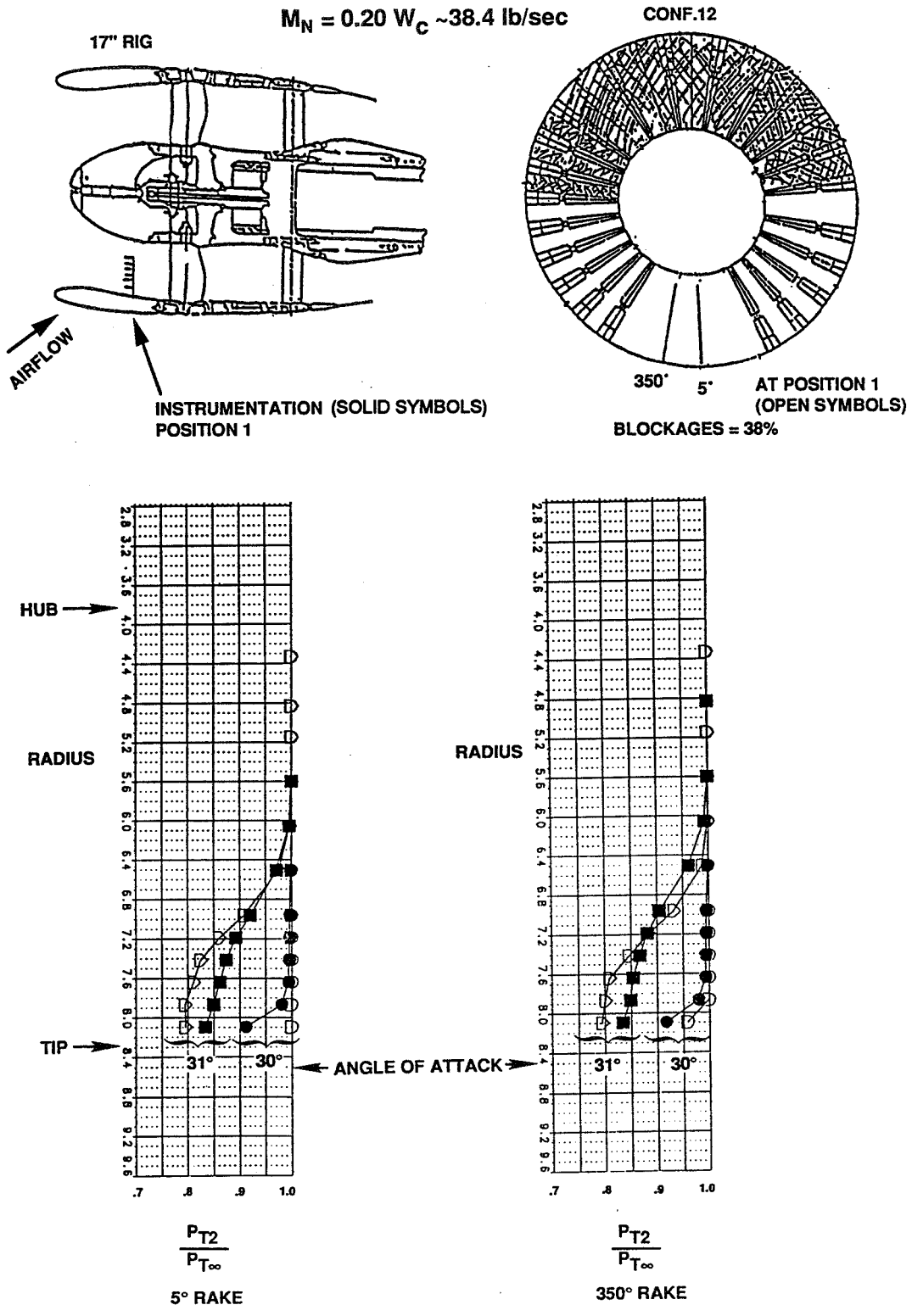

Figure 20 Inlet distortion Not Identical

5.1.3 Data Hysteresis

Data was acquired during the test to evaluate the amount of hysteresis in the inlet separation process. The test section Mach number and model weight flow were held constant. The inlet was pitched up in 1 degree increments until it was fully separated. The angle of attack was then dropped in 1 degree increments until the inlet reattached. Figure 21 shows the inlet static pressure distributions during the run. The inlet was partially separated at 28 degrees angle of attack and fully separated at 29 degrees. As the angle was dropped, the inlet remained fully separated at 28 degrees and did not reattach until 27. Figure 22 further illustrates the hysteresis by showing that the inlet distortion level at 28 degrees angle of attack was dependent on the direction of angle increase.

5.2 PLUG INLET – WITH AND WITHOUT FAN BLOCKAGE

The plug inlet was tested as a flow–through configuration (instrumentation only) and with a combination of rods and screens (38% blockage). This configuration had the most impact on redistributing the flow. The blockage selection was based on the baseline inlet results where the best agreement with the 17" fan rig was achieved. The plug inlet with rods and screens increased separation angle of attack 5 to 6 degrees relative to no blockage (Figure 23). No comparison to the 17" fan rig was made since separation was not achieved with the 17" rig at the largest possible test angle of attack which was 36 degrees. This suggests that the fan presence has a stronger influence on inlet separation for an external plug inlet than for a conventional internal spinner design.

The plug inlet demonstrates the capability to operate to much larger angles of attack than the conventional inlet prior to separation (Figure 24). This capability is highly desirable, but data from other high speed tests indicates there may be high speed performance penalties that would need to be overcome.

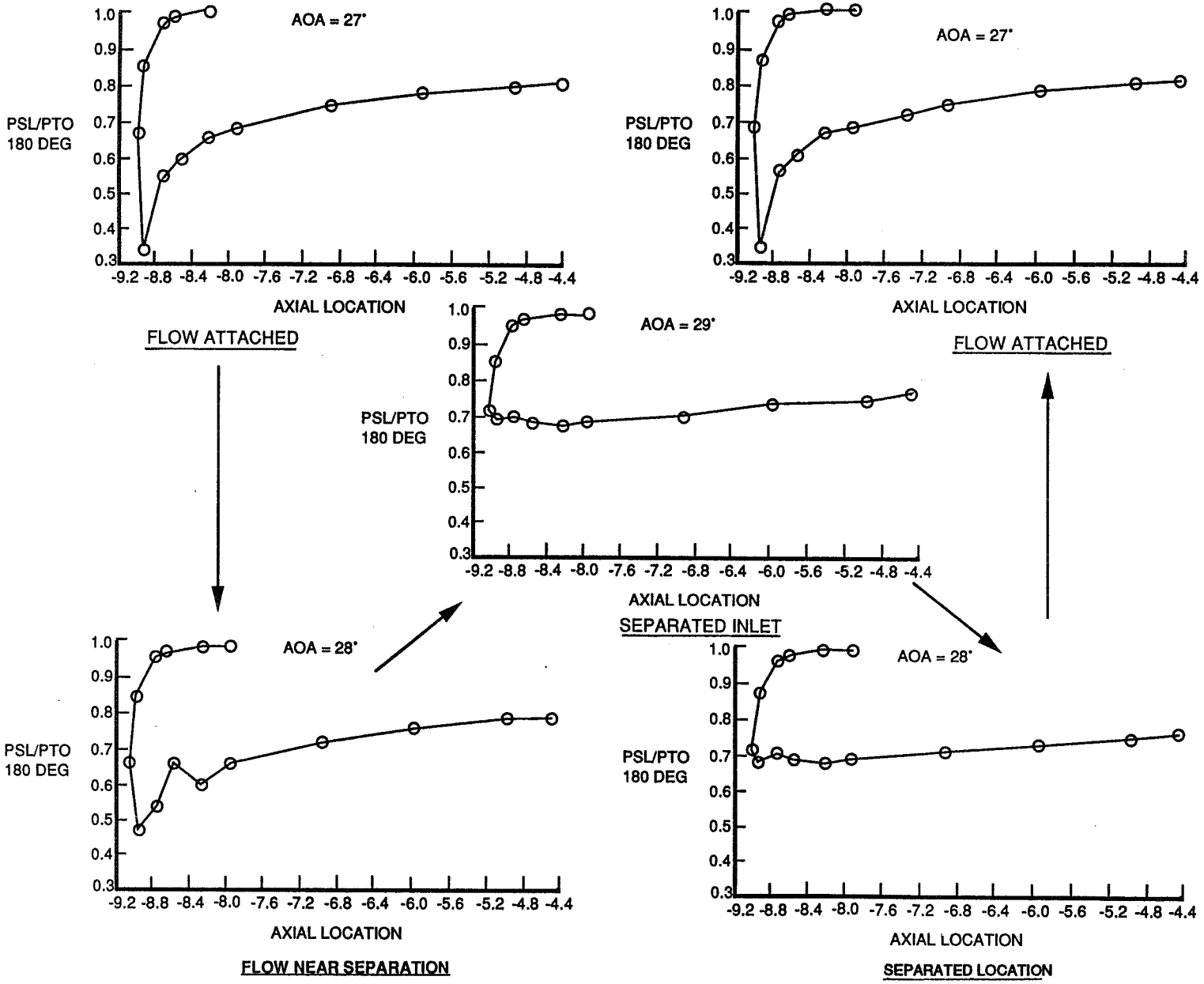

Figure 21 Inlet Separation Hysteresis Was Observed

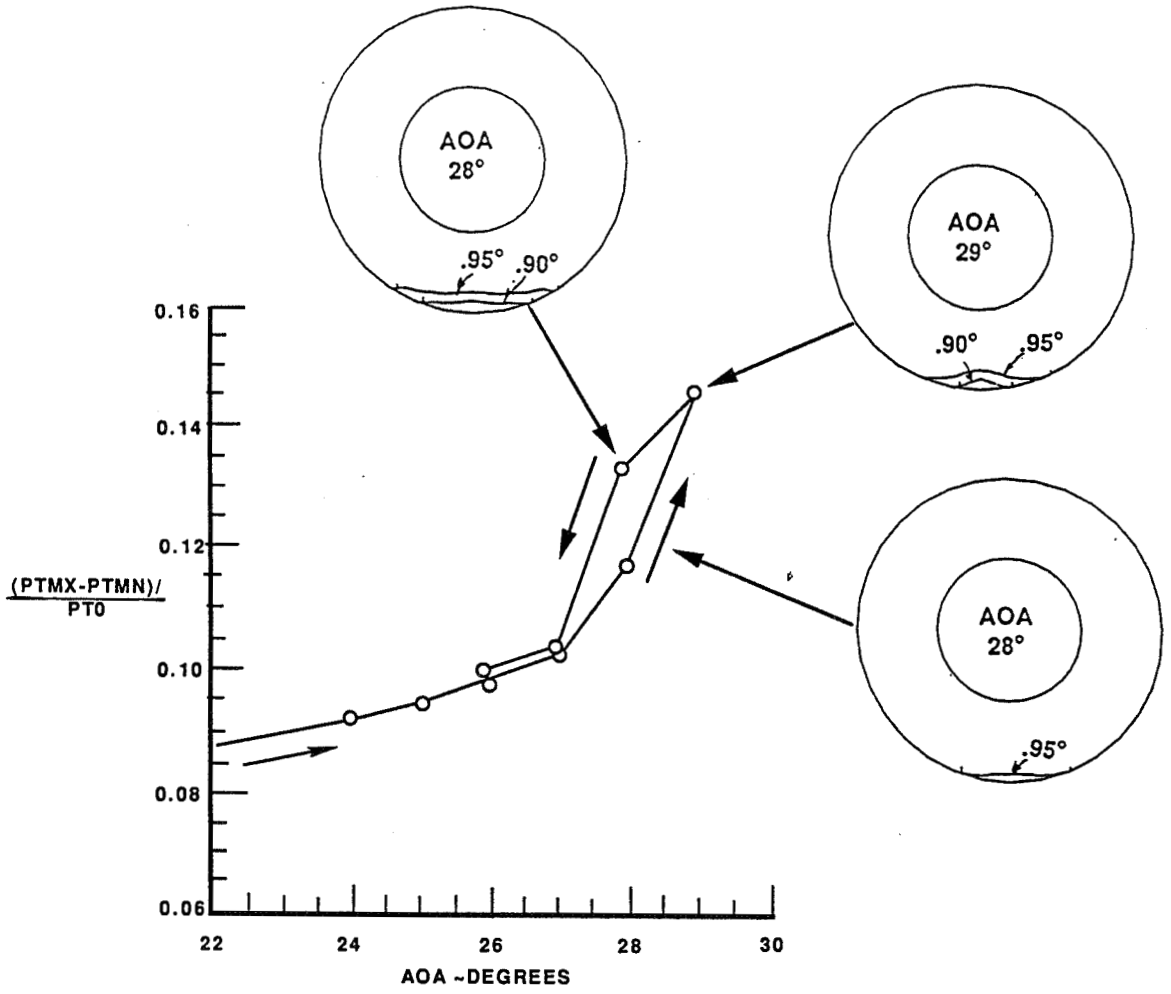

Figure 22 *Inlet Distortion Data Confirms Hysteresis*

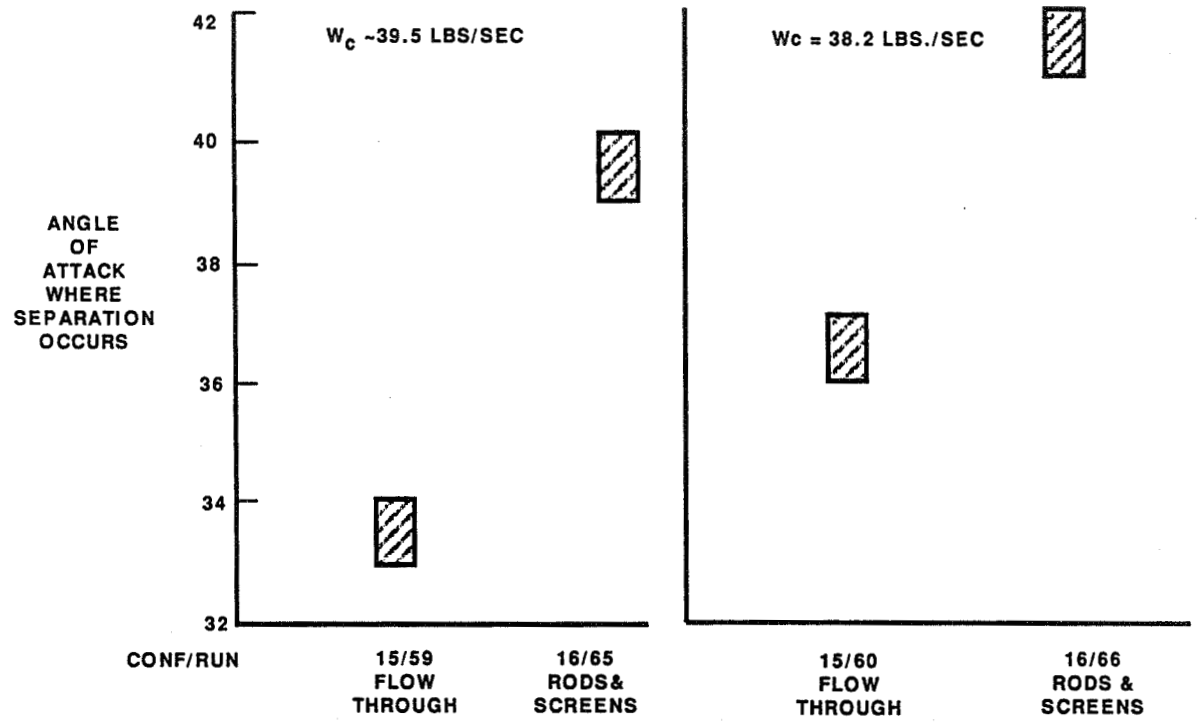

Figure 23 *Plug Inlet With Rod and Screens Increased Separation Angle of Attack 5° to 6° Relative to No Blockage*

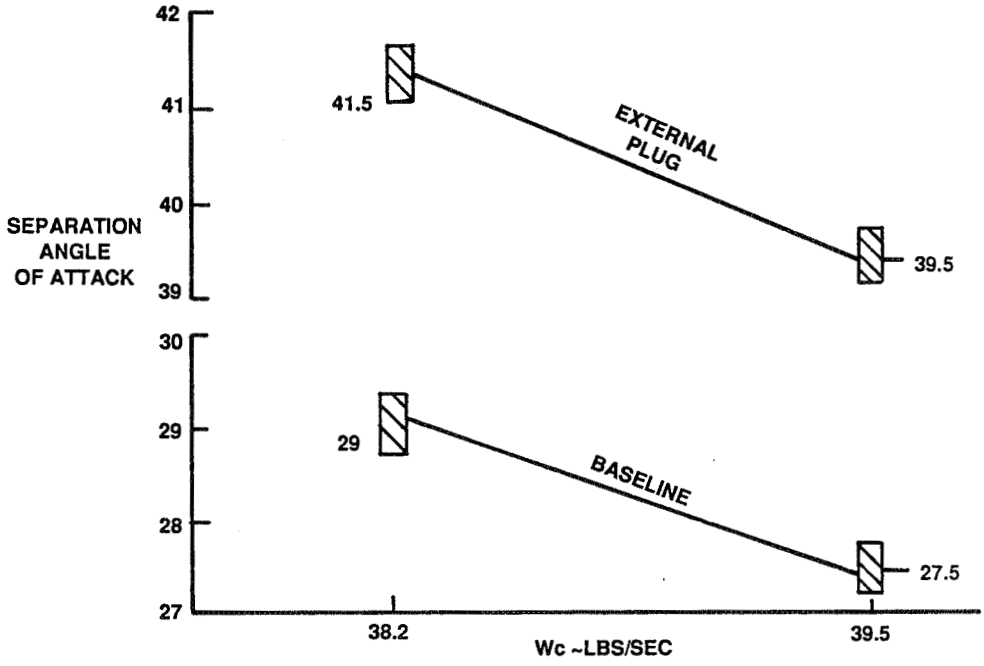

Figure 24 *Plug Inlet Operated to Much Larger ADA Than Baseline Prior to Separation (Rods and Screens).*

6. VORTEX GENERATOR TESTS

6.1 VORTEX GENERATOR DESCRIPTION

A series of vortex generators and trip strips were tested on the conventional inlet to determine their effectiveness on reducing fan face distortion and increasing inlet separation angle of attack capability. As the flow passes over the generators, vortices that energize the flow and help keep the flow attached are produced. Through the use of Euler and strip boundary layer analysis, the size and location of the vortex generators were determined. The Euler results were used to find the locations of the stagnation and minimum pressure points along the inlet contour, with the vortex generators to be located in between these points. The local boundary layer thickness (δ) was determined to be approximately 0.025". Normally "low profile" vortex generators in an application such as control of boattail separation drag would be sized at some fraction of the local boundary layer height. In the present case of inlet lip separation (at model scale), the boundary layer in the region between the stagnation point and the minimum pressure point is extremely thin, and it would have been difficult to accurately fabricate and install discrete vortex generators sized at a fraction of (δ). Therefore, since the intent of these tests was to explore first order effects, it was decided to test two vortex generator heights, equal to and twice the boundary height. Two locations, at the highlight and between the highlight and the stagnation point on the external cowl were evaluated. In addition, the vortex generators were oriented both forward (wedge) and backward (plow) to the oncoming flow. Figure 25 shows the intended impact of vortex generator orientation. As a wedge, the vortices tend to lift off the flow surface and as a plow they stay near the surface and reverse the direction of vortex rotation.

Finally, a trip strip approximately half the boundary height (0.010") was placed at the highlight. Figures 26 and 27 provide a description and location of the vortex generators and trip strip. It should be noted that the vortex generators were spaced 0.33 inches apart, centerline to centerline, over the bottom $\pm$45 degrees of the inlet for the 0.055 inch height vortex generator and 0.25 inches apart for the 0.025 inch VG. (S/h in the range 6 to 10).

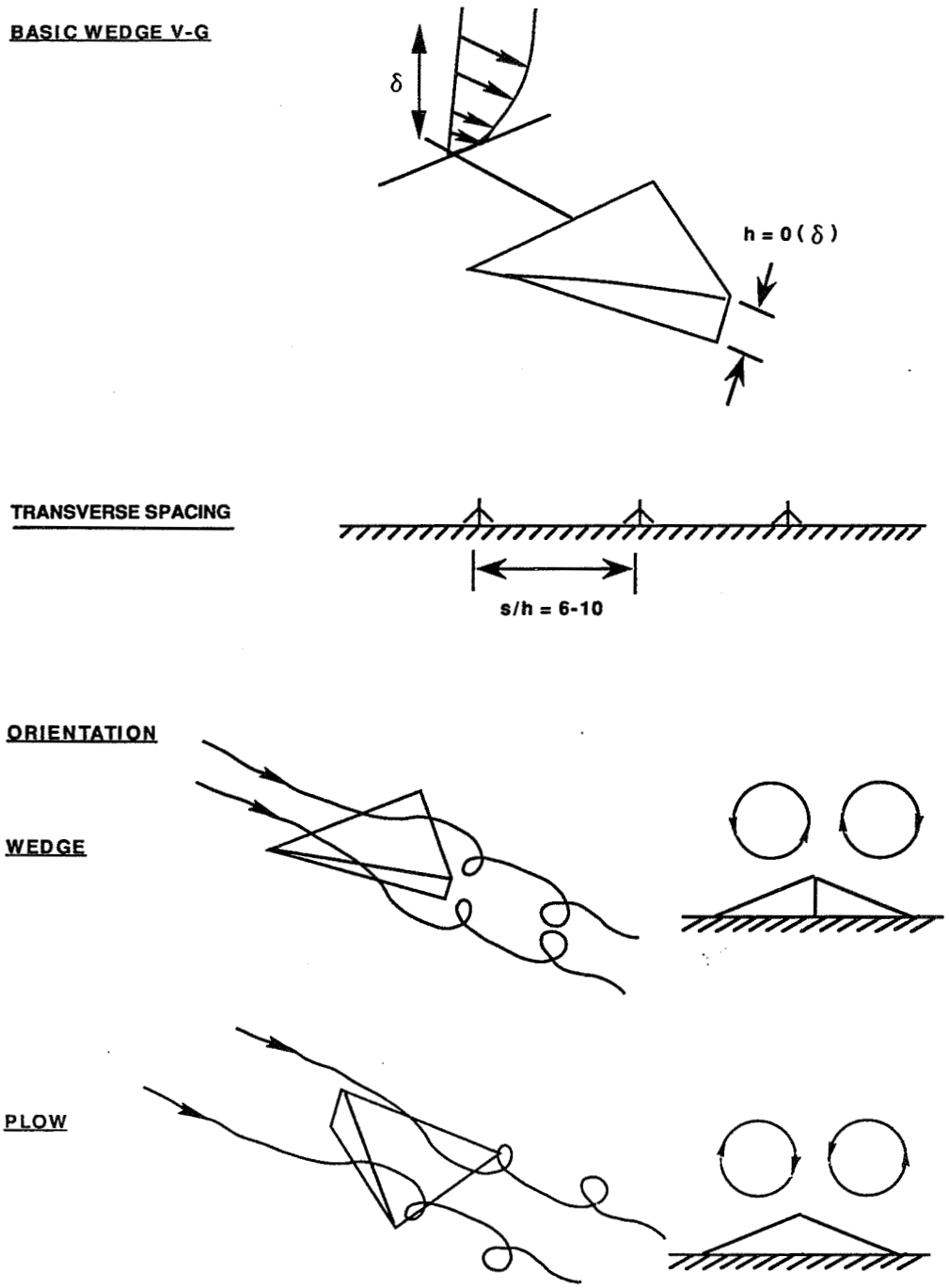

Figure 25 Downstream View Looking Upstream

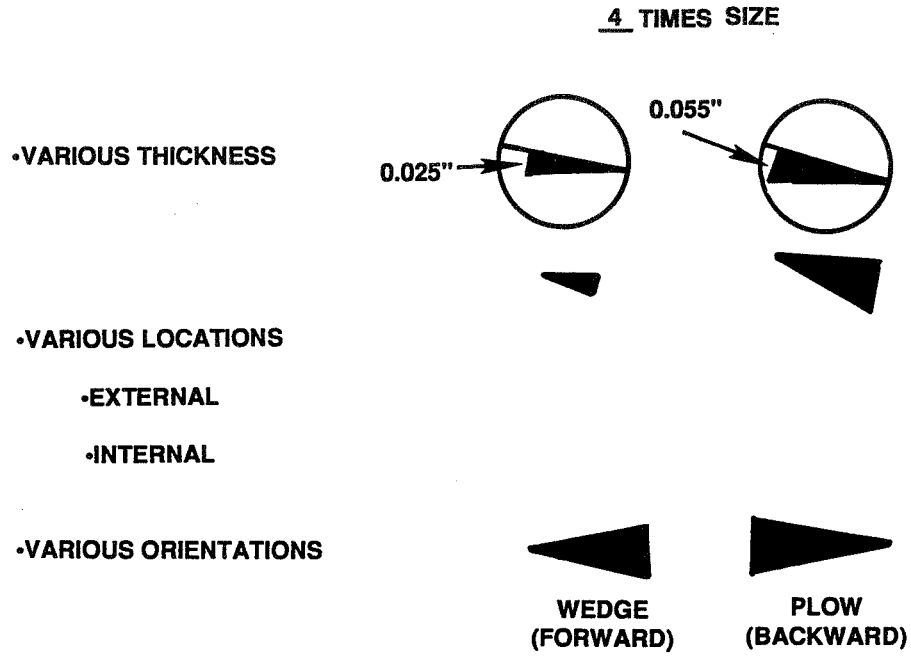

Figure 26 *A Series of Vortex Generators Were Tested to Determine Their Effectiveness for Reducing Inlet Distortion and Increasing Angle of Attack Capability*

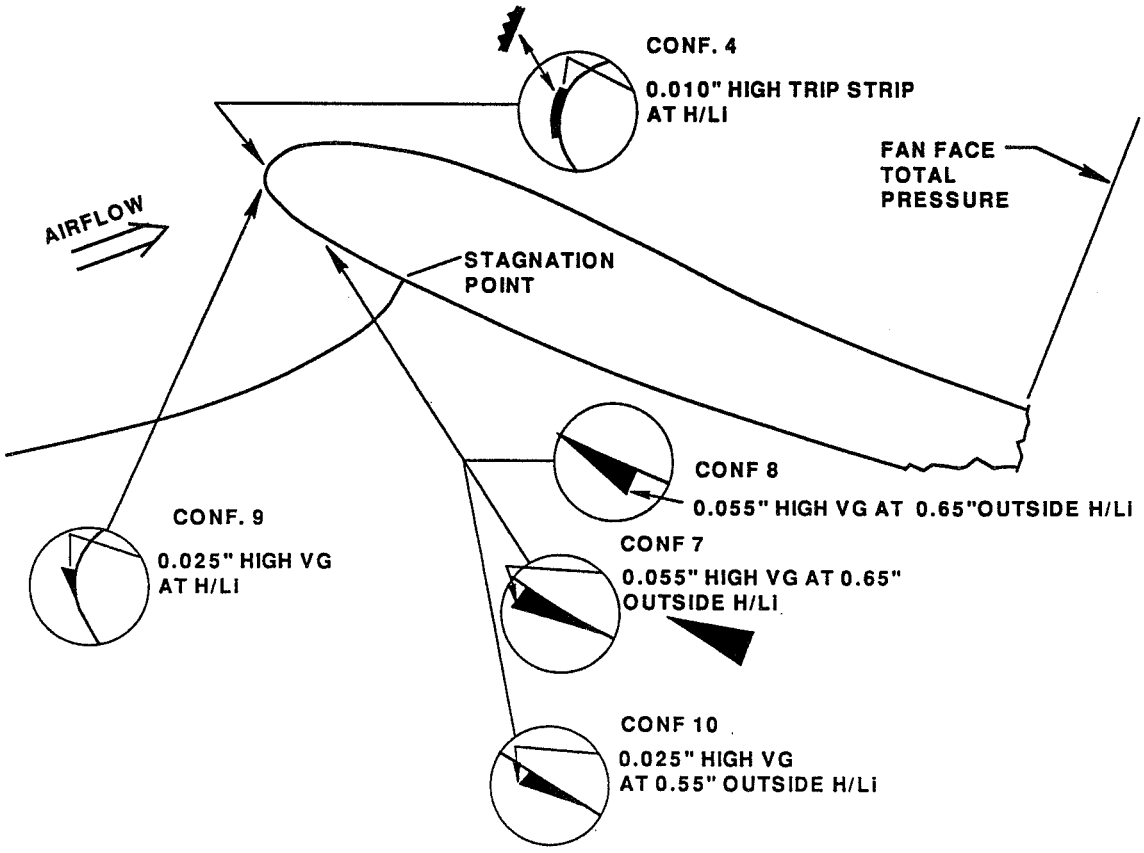

Figure 27 *Vortex Generator Descriptions*

6.2 TEST RESULTS

All configurations were run at take off conditions varying the angle of attack from 0 to 31 degrees. The results are shown in Figures 28 and 30. Vortex generators and trip strips generally increased the inlet angle of attack capability. The 0.010" high trip strip located at the highlight increased the angle of attack before separation of 2 degrees while forward facing vortex generators (0.055" and 0.025" high) located on the external contour 0.055" aft of the highlight achieved an increase of 1 degree over the baseline. Rearward facing vortex generators and those placed at the highlight had the same angle of attack as the baseline.

At an inlet angle of attack of 27 degrees, the inlet flow for all configurations was attached. Figure 29 shows the distortion measured at this angle. The vortex generators positioned outside the hi−lite and the trip strip did not significantly increase the total pressure distortion measured as compared to the baseline configuration. The Pt/Pto values at 95% span ranged from 0.91 to 0.925 with the baseline falling at 0.92. The configuration with the 0.025" vortex generator at the hi−lite caused more distortion than any other configuration with a Pt/Pto value of 0.845 at 95% span.

The high amounts of distortion caused by the vortex generator at the hi−lite may be the result of improper sizing or placement of the device. From Euler Analysis, the boundary layer thickness and local Mach number at the hi−lite were expected to be on the order of 0.010" and 1.5, respectively. The use of the 0.025" vortex generators coupled with the high local Mach number at the hi−lite might cause the high loss of total pressure that is shown in Figure 29.

Configurations other than the vortex generator at the hi−lite consisted of vortex generators that were on the same order as the boundary layer thickness and/or in regions of lower local Mach numbers. These configurations resulted in total pressure distortion on the order of the baseline configuration for the attached inlet condition.

Figure 30 shows distortion measurements at the fan face for an inlet angle of attack of 30 degrees. At this angle, the inlet was separated for all configurations. The baseline and the configuration with vortex generators at the hi−lite demonstrated similar Pt/Pto results. The trip strip and vortex generators positioned outside the hi−lite showed less distortion than the baseline across the entire span. The baseline Pt/Pto value of 0.87 at 80% span compared to the Pt/Pto value of 0.90 at 80% span for the trip strip and vortex generators outside the hi−lite. At other span points, the trip strip showed as much as a 0.04 Pt/Pto improvement over the baseline case, while the vortex generators outside the hi−lite improved by as much as 0.03 Pt/Pto over the baseline.

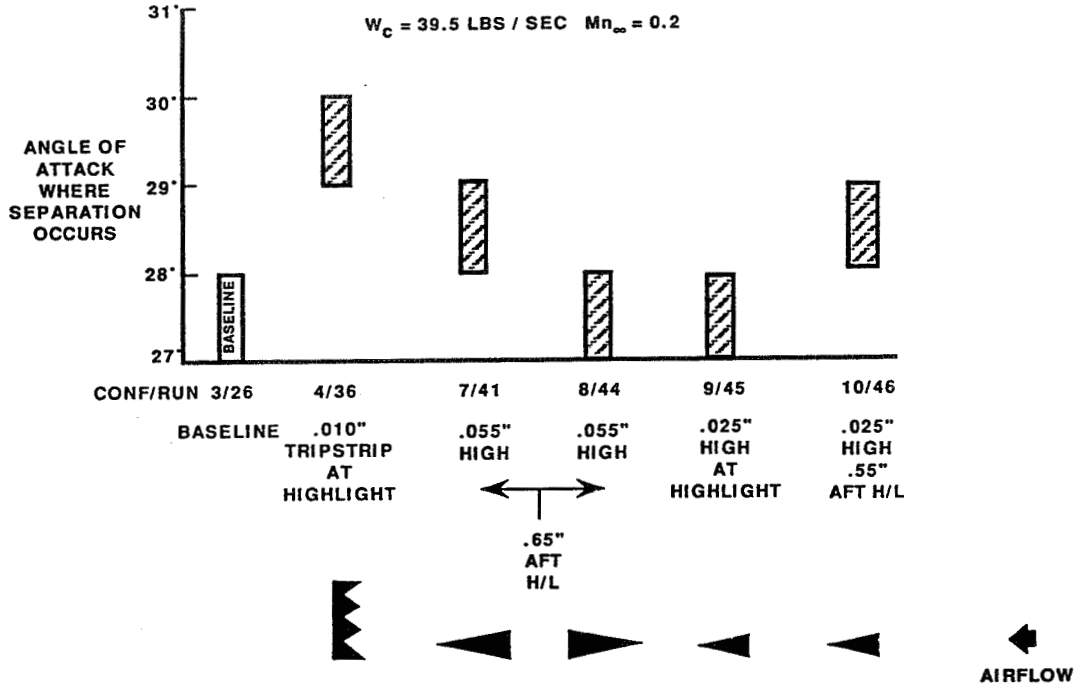

Figure 28 *Vortex Generators and Trip Strips Increase Angle of Attack Capability*

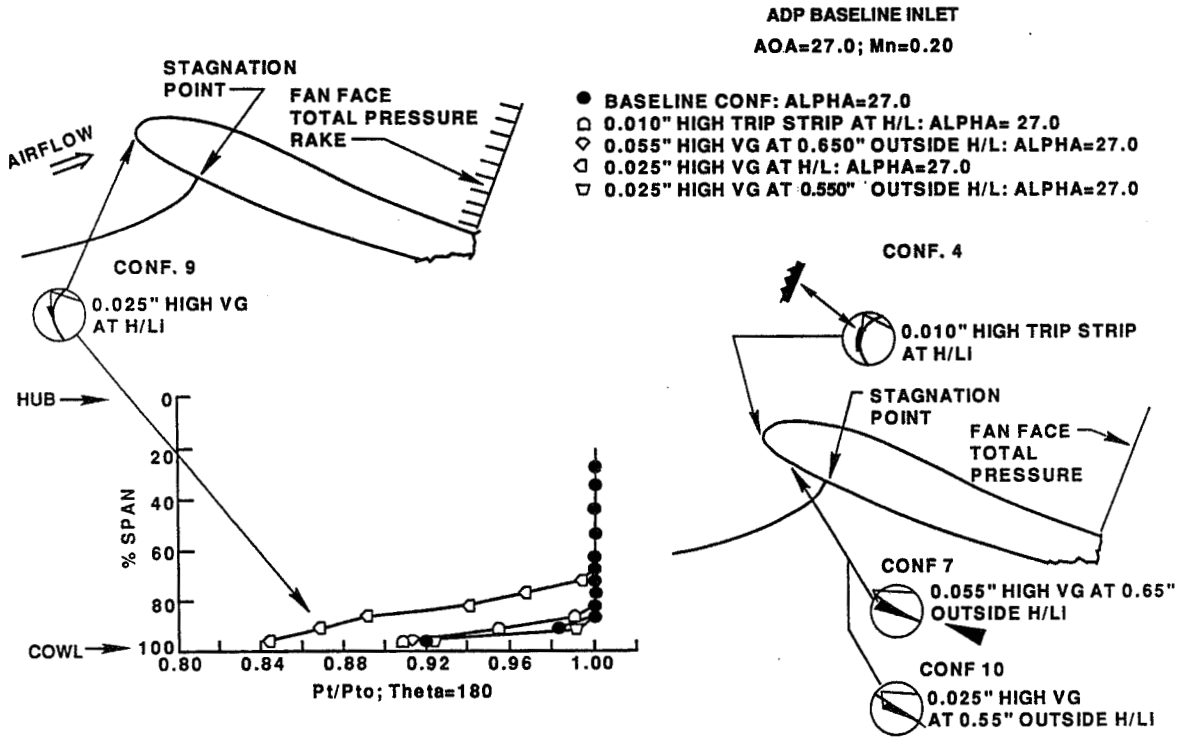

Figure 29 *Vortex Generators Positioned At the Highlight Increased Fan Face Total Pressure Loss With Separation Free Inlet*

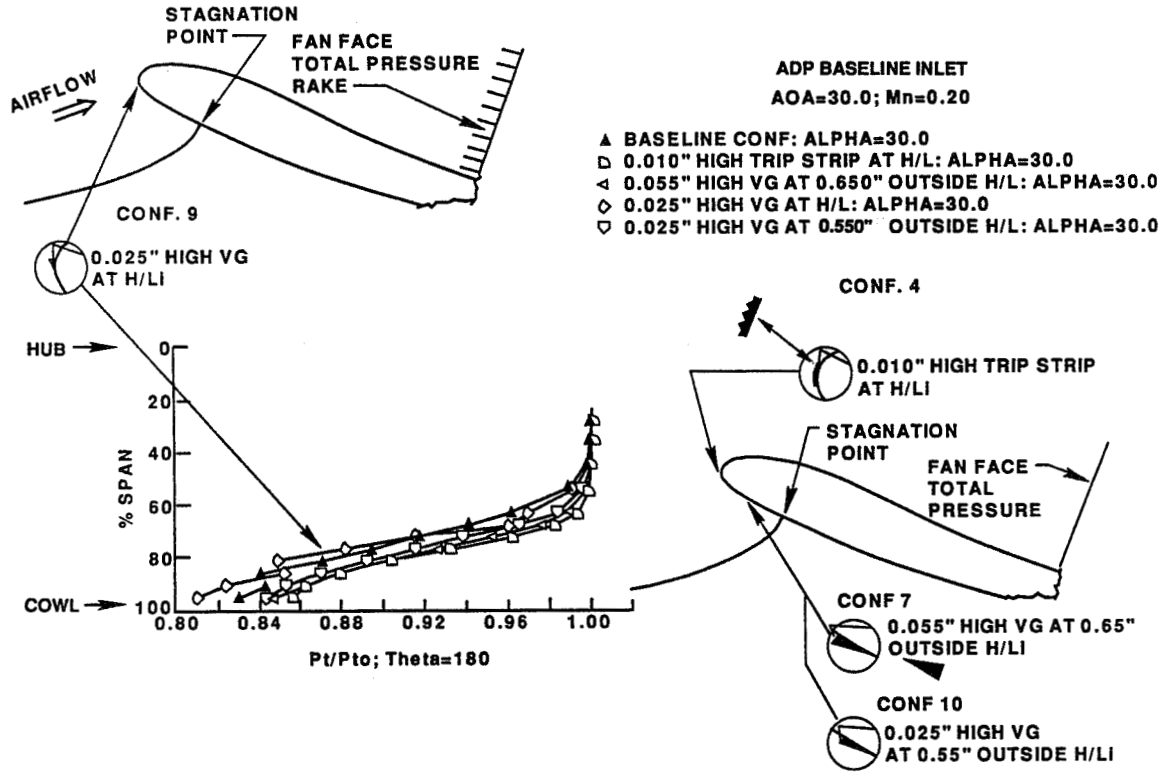

Figure 30 *Separated Inlet Distortion Is Highest for Vortex Generators Located At Highlight and Lowest for Trip Strip*

7. PROPOSED FAN BLOCKAGE SIZING METHOD

Data shows that proper combinations of screens and rods are capable of producing through–flow angle of attack (AOA) results that duplicated the 17" fan model data. While the separated total pressure hole with screen blockage was deeper than for the case with a fan, the circumferential width of the distortion pattern was similar. The question we now face is, "Do we understand the results well enough and have the tools to make the design of blockage patterns (combination of rods and screens) a controlled and repeatable process?" This capability would provide an alternative, inexpensive test approach to determining inlet separation and distortion characteristics without testing with a fan.

The proposed fan blockage sizing method, shown in Figure 31, begins with estimating inlet distortion levels anticipated for new inlet and fan designs. The distortion is a function of operability requirements (such as angle of attack, crosswind capability or evasive maneuvers) airflow and inlet geometry. Distortion/geometry, airflow correlations can be developed using the recently acquired data. The next step would be to determine the static pressure distortion at the fan face using a strip compressor calculation that includes a fan and an inlet distortion map. The strip compressor calculation can model Mach numbers in each sector of the inlet with a match of fan downstream static pressure behind a fan characteristic. As a result, a delta static pressure between the clean and distorted sectors is produced. The calculation can be rerun without a fan but with a blockage loss to redistribute flow, force flow into the distorted area and allow larger delta static pressure which reflects a flow redistribution. By imposing various levels of loss based on screen size and porosity from the recent test, the level of delta static pressure for the case with the fan can be reproduced. Items that are not included in this one dimensional system are the streamline curvature associated with redistribution of flow and the mixing attenuation of the static pressure with inlet length. Once the blockage loss is established, a blockage loss calculation can be used to determine screen design. It should be noted that it is possible to have more than one combination of rods and screens for a given level of loss. The test data from this test can be used to calibrate this process. It can be seen from Figure 32 that the blockage test results show there is a more severe static pressure delta (between the clean and distorted sectors) than the 17" powered fan results. This would suggest that further tailoring of the rods and screens may produce the same pressure data seen with the 17" fan, however, a calibrated blockage sizing method would be needed in order to tailor the rods and screens.

STEP

1) ESTIMATE INLET DISTORTION LEVELS (MAPS) ANTICIPATED FOR NEW INLET & FAN DESIGN

DISTORTION IS A FUNCTION OF: 1) OPERABILITY REQUIREMENT
- ANGLE OF ATTACK
- CROSSWIND
- EVASIVE MANEUVER (WIND UP TURN)

2) AIRFLOW ~ $\dot{W}c/A_{FAN\ FACE}$

3) INLET GEOMETRY

} EXPAND EXISTING GEOMETRY/DISTORTION CORRELATIONS USING RECENTLY ACQUIRED DATA

2) USING INPUT FROM STEP (1) DETERMINE STATIC PRESSURE DISTORTION AT FAN FACE USING A STRIP COMPRESSOR CALCULATION THAT INCLUDES FAN

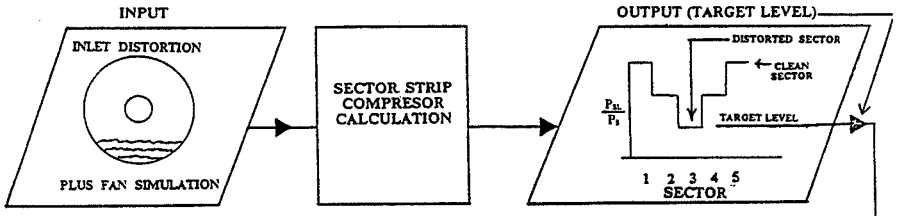

NOTE: P_{SL} IS THE LOCAL STATIC PRESSURE AND P_S IS THE STATIC PRESSURE LEVEL IN THE CLEAR SECTION

3) RERUN STRIP COMPRESSOR CALCULATION (WITHOUT FAN) WITH BLOCKING LOSS

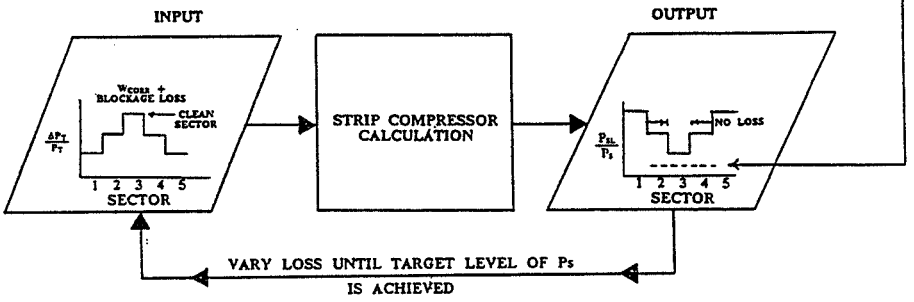

4) ONCE BLOCKAGE LOSS IS ESTABLISHED USE BLOCKAGE LOSS CALCULATION TO DETERMINE SCREEN DESIGN

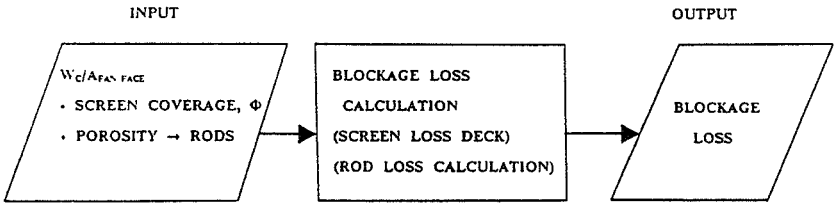

NOTE: IT'S POSSIBLE TO HAVE MORE THAN 1 COMBINATION OF RODS & SCREENS FOR A GIVEN LEVEL OF LOSS

5) USE TEST DATA TO CALIBRATE PROCESS

GO BACK TO STEP 1 WITH DATA TO CONFIRM INITIAL ESTIMATES

Figure 31 Proposed Fan Blockage Sizing Method

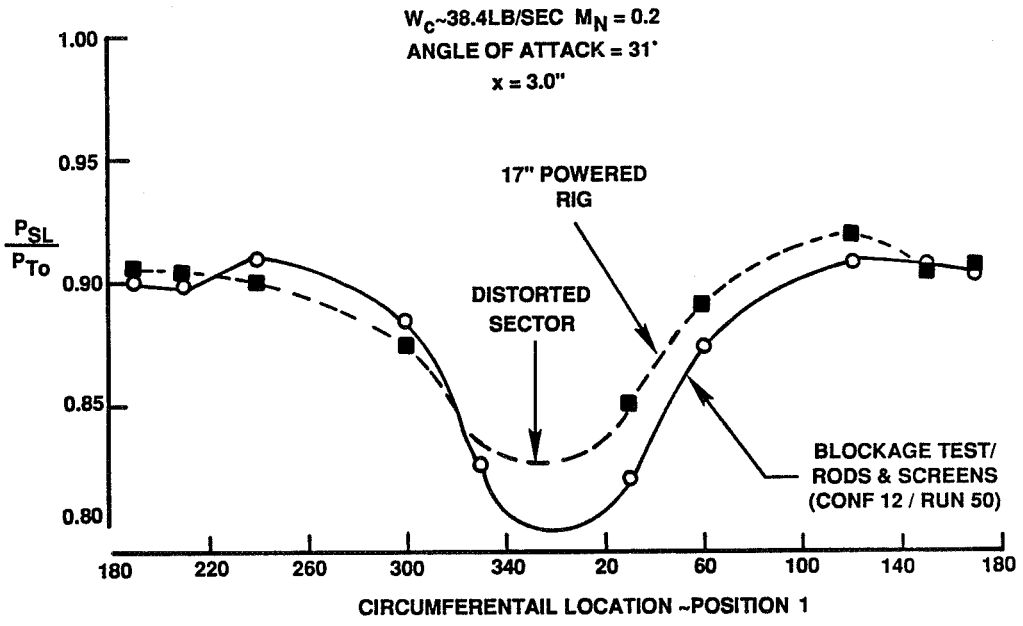

Figure 32 *Separated Inlet Produces Circumferential Static Pressure Distortion*

8. CONCLUSIONS AND RECOMMENDATIONS

- Presence of fan increased separation free angle of attack operation 3 to 4 degrees relative to what flow–through data would indicate.
- Care must be taken with inlet instrumentation rakes since they can contaminate the data. Instrumentation poles in the inlet diffuser can increased (apparent) separation free operation 2 degrees in angle of attack in this experiment which had to be corrected out of the results.
- Flow blockage can simulate fan aero impact on inlet separation angle of attack. The Mach number through the blockage should be 0.8 or greater. Tailored circumferential blockage patterns were slightly better when maximum blockage was located in top quadrant and there was no blockage on the bottom quadrant.
- Future separation angle of attack determination testing can be done with blockage devices but with inlet instrumentation removed. Surface pressures and fan face distortion can be used to determine onset of separation.
- Future total pressure distortion testing should be conducted with a fan. The separation total pressure hole was demonstrated with blockage. The total pressure depression was deeper.
- Trip strips and vortex generators can be effective and they should be located outside of highlight and ahead of stagnation streamline. Results were insensitive to size (therefore use smaller).
- It is recommended that a fan simulation design method for total pressure pattern simulation be developed and verified with a test of a new fan and inlet design.

9. REFERENCES

1. Overall, B. W.: "A Procedure for the Design of Complex Distortion Screen Patterns for Producing Specified Steady–State Total Pressure Profiles at the Inlet of Turbine Engines," AEDC–TR–72–10 Report Dated January 1972.

2. Wood, C. C. and Knip, G.: "An Investigation of Screens for Removing Distortions Induced Flows At High Subsonic Speeds," NASA RM L 57608 Dated September 26, 1957.

APPENDIX A

DATA REDUCTION EQUATIONS

Mass Averaged Total Pressure

$$PsRake\ (I,J) = \left[\frac{PsFFO(I) - PsFFI(I)}{4.7704}\right] * (RAD(I,\ J) - 3.8269) + PsFFI(I)$$

I – Rake

J – Probe

$$MnRake(I,J) = \left[5 * \left[\left(\frac{PsRake(I,J)}{P_T(I,J)}\right)^{-2/7} - 1\right]\right]^{1/2} \qquad MnRake(I,J) = \left[5 * \left[\left(\frac{PsRake(I,J)}{P_{TBL}(I,J)}\right)^{-2/7} - 1\right]\right]^{1/2}$$

$$M_{DOT}\ (I,J) = MnRake(I,J)\left(1 + \frac{\gamma - 1}{2}\ (MnRake(I,J))^2\right)^{1/2}$$

$$Sum = \sum_{I=1}^{4}\ \sum_{J=1}^{12}\ PsRake(I,J) * M_{DOT}(I,J) * A(I,J)$$

$$+ \sum_{I=1}^{4}\ \sum_{J=1}^{9}\ PsRake(I,J) * M_{DOT}(I,J) * A(I,J)$$

$$PTMass = \left[\sum_{I=1}^{4}\left(\frac{PsFFO(I) + P_T(I,1)}{2}\right) * PsRake(I,1) * M_{DOT}(I,1) * A(I,1) \quad +\right.$$

$$\sum_{I=1}^{4}\left(\frac{PsFFO(I) + P_{TBL}(I,1)}{2}\right) * PsRake(I,1) * M_{DOT}(I,1) * A(I,1) \quad +$$

$$\sum_{I=1}^{4}\sum_{J=2}^{12} PT(I,J) * PsRake\ (I,J) * M_{DOT}(I,J) * A(I,J) \quad +$$

$$\left.\sum_{I=1}^{4}\sum_{J=2}^{9} P_{TBC}(I,J) * PsRake(I,J) * M_{DOT}(I,J) * A(I,J)\right]$$

$$PtMAFF = PtMASS/SUM$$

Area Averaged Total Pressure

$$SUMFF = \sum_{I=1}^{4}\sum_{J=1}^{12} A(I,J) + \sum_{I=1}^{4}\sum_{J=1}^{9} A(I,J)$$

$$P_{TAAFF} = \frac{\left[\sum_{I=1}^{4}\sum_{I=1}^{12} P_T(I,J) * A(I,J) + \sum_{I=1}^{4}\sum_{J=1}^{9} P_{TBL}(I,J) * A(I,J)\right]}{SUMFF}$$

$$SUMINC = \sum_{I=1}^{4}\sum_{J=1}^{12} A(I,J) + \sum_{I=1}^{4}\sum_{I=1}^{9} A(I,J) + \sum_{I=1}^{10} A(I)$$

$$P\ 2AA = \left[\sum_{I=1}^{4}\sum_{J=1}^{12} P_T(I,J) * A(I,J) + \sum_{I=1}^{4}\sum_{J=1}^{9} P_{TBC}(I,J) * A(I,J) + \sum_{I=1}^{10} Ps10(I) * A(I)\right] \Big/ SUMINC$$

Pressure Coefficients

$$CPAX(I,J) = \frac{P_{SAX}(I,J) - P_{S\phi}}{Q_\phi}$$

Flow Calculations

Analytical Calibration

Conventional Inlet – For All Mach No.

$$X = \left(\sum_{I=1}^{10} P_{T\phi}/Ps\ 10(I)\right) \Big/ 10$$

Z = 2.15

$$WFNASA = \left[(55.7664 ** Z) * \left(1.0 - ((1.4649 - X)/0.4649) ** Z\right)\right] ** (1.0/Z)$$

Plug Inlet

Mn = 0.10 Z = 2.25

$$WFN10 = \left[(52.5 ** Z) * \left(1.0 - ((1.8 - X)/0.8) ** Z\right)\right] ** (1.0/Z)$$

Mn = 0.25 Z = 2.35

$$WFN25 = \left[(52.0 ** Z) * \left(1.0 - ((1.7 - X)/0.7) ** Z\right)\right] ** (1.0/Z)$$

$$WFNASA = \left(M_\phi - 0.10\right)/0.15 * (WFN25 - WFN10) + WFN10$$

$$WFCORR = WFVEN \sqrt{\frac{TT\phi}{518.67}} \left(\frac{14.696}{PT\phi}\right)$$

$$MBARO = 0.918903 * \left(\frac{Ps\phi}{PT\phi}\right) * M\phi * \sqrt{1.0 + \frac{\gamma - 1}{\gamma} (M\phi)^2}$$

$$\gamma = 1.4$$

$$MFR = WCORR \frac{\sqrt{518.67}}{14.696 * MBAR\phi * AHI}$$

Tunnel Reynolds Number/Ft

$$RN\phi = \left(1.8115\ X\ 10^8 * M_\phi * P_{T\phi} * \left(TT\phi * \left(\frac{Ps\phi}{P_{T\phi}}\right) ** 0.28571 + 198.6\right) * \left(\frac{Ps\phi}{P_{T\phi}} * 0.42871\right)\right) \Big/ TT\phi^2$$

Venturi Entrance Conditions

$$P_{TBAV} = \left(\sum_{I=1}^{4} PTBM(I)\right) \Big/ 4$$

$$T_{TBAV} = \left(\sum_{I=1}^{4} TTBM(I) \right) \Big/ 4$$

Venturi Flow Coefficient

$P_{TBAV}/P_{sThroat} < /0.232$

$C_D = 0.3882237 + 0.6073032\ (P_{TBAV}/P_{sThroat})$

$1.0232 < P_{TBAV}/P_{sThroat} < 1.1044$

$C_D = -.159431 + 2.141464\ (P_{TBAV}/P_{sThroat}) - 0.9758157\ (P_{TBAV}/P_{sThroat})^2$

$P_{TBAV}/P_{sThroat} > 1.1044$

$C_D = 1.01540$

Distortion Parameters

$$\text{IDIST } \phi = \frac{P_{TIMAX} - P_{TIMIN}}{P_{T\phi}}$$

$$\text{IDIST 1} = \frac{P_{TIMAX} - P_{TIMIN}}{P_{T2AA}}$$

$$\text{IDIST 2} = \frac{P_{TIMAX} - P_{TIMIN}}{P_{TMAFF}}$$

Recovery Factors

$$\text{IRAM1} = P_{2AA}/PT\phi$$

$$\text{IRAMA2} = P_{TAAFF}/PT\phi$$

$$\text{IRAMM2} = P_{TMAFF}/PT\phi$$

APPENDIX B

INSTRUMENTATION DEFINITION

Position 2.0
(Fan Face Station)

Inlet Total Pressures

Plug and Conventional

i	x = -0.411 w/o kulite R	x = -0.411 w/kulite R
12	4.617	5.116
11	5.116	5.433
10	5.433	5.886
9	5.886	6.340
8	6.340	6.793
7	6.793	7.019
6	7.246	7.246
5	7.473	7.473
4	7.699	7.699
3	7.926	7.926
2	8.153	8.153
1	8.379	8.379

j	UTRC Setup	NASA Setup
A	5	5
B	140	350
C	180	180
D	200	200

Position 2.0
(Fan Face Station)

Inlet Boundary Layer Total Pressures

Plug and Conventional

x = -0.411

i	R
9	7.606
8	7.806
7	8.006
6	8.166
5	8.296
4	8.396
3	8.466
2	8.516
1	8.556

j	UTRC Setup	NASA Setup
C	90	90
E	160	160
F	225	225
H	350	20

Position 2.0
(Fan Face Station)

Fan Face Static Pressures

Inner and Outer Wall

Inner Wall x = -0.411
Outer Wall x = -0.767

i	
1	2.0
2	24.75
3	61.4
4	94.0
5	131.4
6	156.0
7	184.0
8	221.0
9	263.9
10	311.0

Position 2.0
(Fan Face Station)

Total Pressure Rake Static Pressure Assignments for Mass Averaged Total Pressure Calculation

Rake	UTRC Setup PSFFI(i)	UTRC Setup PSFFO(i)	NASA Setup PSFFI(i)	NASA Setup PSFFO(i)
A	1	1	1	1
B	5	5	1	1
C	7	7	7	7
C(Boun. Lay.)	4	4	4	4
D	7	7	7	7
E	6	6	6	6
F	8	8	8	8
H	1	1	2	2

Position 1
Inlet Surface Static Pressures (PS20-j)

X = -3.016 (Conventional)
X = -2.402 (Plug)

j	____
A	30°
B	60°
C	120°
D	150°
E	170°
F	190°
G	210°
H	240°
J	300°
K	330°

POSITION 1

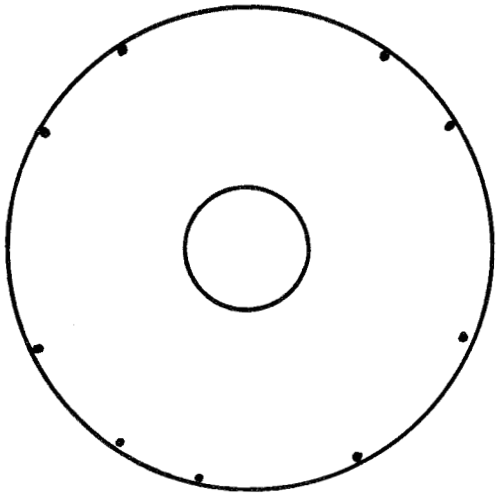

Note: The circumferential coordinate system is defined 0° = TDC, counter-clockwise, looking upstream

Note: The axial coordinate system is identified at the blade stacking line (X=1.21).

Position 1
Inlet Total Pressures (P2-ji)

j	
A	5°
B	140°
C	180°
D	200°

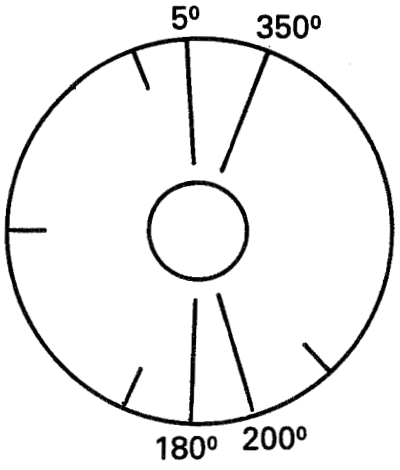

NASA SETUP

Coventional

X = -3.016

w/o kulite R	w/kulite R
4.333	4.833
4.833	5.150
5.150	5.603
5.603	6.057
6.057	6.510
6.510	6.736
6.963	6.963
7.190	7.190
7.416	7.416
7.643	7.643
7.870	7.870
8.096	8.096

Note: Close-coupled transducers tied to sensors B4 & B10.

Note: The axial coordinate system is identified at the blade stacking line (X = 1.21).

Position 1
Inlet Boundary Layer Total Pressures (PBL2-ji)

j	____	Conventional X = -3.016 R
C	90°	7.323
E	160°	7.523
F	225°	7.723
H	350°	7.883
		8.013
		8.113
		8.183
		8.233
		8.273

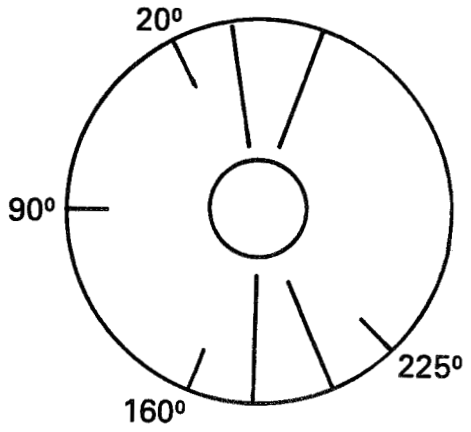

NASA SETUP

Note: The circumferential coordinate system is defined 0° = TDC, counter-clockwise, looking upstream.

Note: The axial coordinate system is identified at the blade stacking line (X=1.21).

Position 1
Inlet Surface Static Pressures (52) (PSIN-ji)
(Conventional)

j	Θ	i	X (inner surface)	i	X (outer surface)
A	99°	1	-1.33	16	-7.5
D	341° 15'	2	-2.0	15	-8.2
		3	-3.0	14	-8.6
		4	-3.5	13	-8.8
		5	-4.5	12	-9.0 (offset .188)
		6	-5.0	11	-9.068 (hilite)
		7	-6.5		
		8	-8.0		
		9	-8.6		
		10	-9.0 (offset .188)		

j	Θ	i	X (inner surface)	i	X (outer surface)
B	168° 15'	1	-1.33	18	-8.0
		2	-2.0	17	-8.3
		3	-3.0	16	-8.6
		4	-4.5	15	-8.8
		5	-5.0	14	-9.0 (offset .188)
		6	-6.0	13	-9.068 (hilite)
		7	-7.0		
		8	-8.0		
		9	-8.3		
		10	-8.6		
		11	-8.8		
		12	-9.0 (offset .188)		

j	Θ	i	X (inner surface)
C	286°	1	-1.33
		2	-2.0

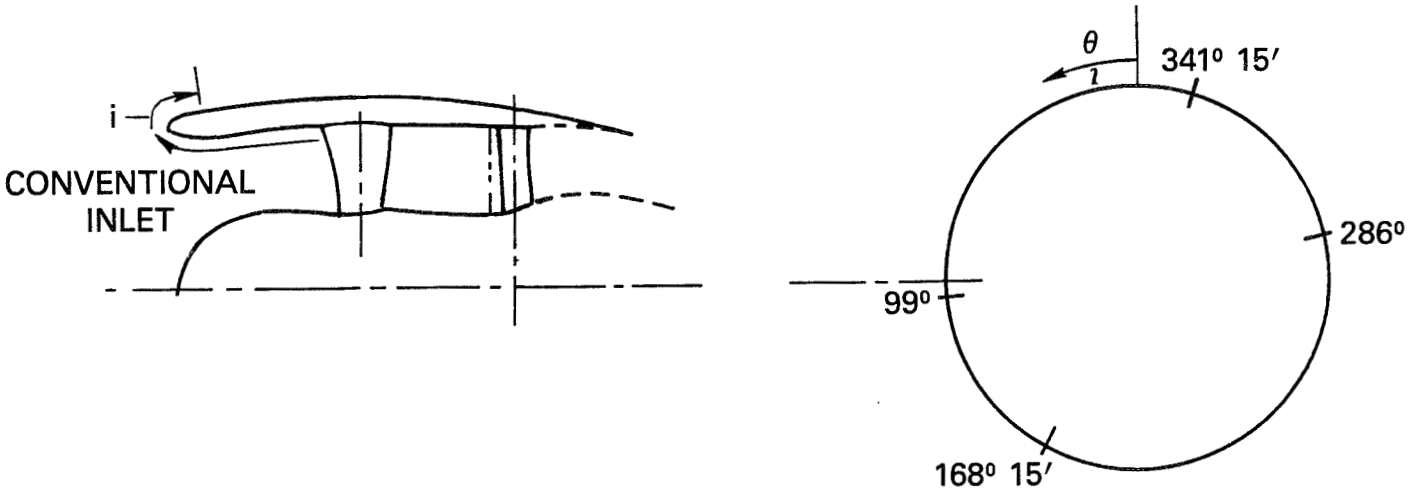

Note: The circumferential coordinate system is defined 0° = TDC, counter-clockwise, looking upstream .

Note: The axial coordinate system is identified at the blade stacking line (X=1.21).

Additional Inlet Surface Static Pressures (PSIN-ji)
(Conventional)

j	____	i	X (inner surface)	i	X (outer surface)
E	180°	1	-4.50	15	-8.0
		2	-5.0	14	-8.3
		3	-6.0	13	-8.7
		4	-7.0	12	-8.8 (offset .125)
		5	-8.0	11	-9.0 (offset .125)
		6	-8.3	10	-9.068 (hilite)
		7	-8.6		
		8	-8.8		
		9	-9.0		

j		i	x (inner surface)	i	x (outer surface)
F	0	1	-4.50	12	-8.00
		2	-5.00	11	-8.30
		3	-6.00	10	-8.70
		4	-7.00		
		5	-8.00		
		6	-8.30		
		7	-8.60		
		8	-8.80		
		9	-9.00		

Note: The circumferential coordinate system is defined 0° = TDC, counter-clockwise, looking upstream.

Note: The axial coordinate system is identified at the blade stacking line (X=1.21).

Inlet Surface Static Pressures (38) (PSIN-ji)
(Plug)

j	θ	i	X (inner surface)	i	X (outer surface)
		1	-1.33	12	-2.0
D	341° 15'	2	-2.0	11	-2.4
		3	-2.4	10	-2.8
		4	-2.8	9	-3.4 (offset.3125)
		5	-3.4 (offset .188)	8	-3.5 (offset.3125)
		6	-3.5 (offset .188)	7	-3.55 (hilite)

j		i	x (inner surface)	i	x (outer surface)
F	0	1	-2.80	8	-2.80
		2	-3.10	7	-3.40
		3	-3.40	6	-3.50
		4	-3.50		
		5	-3.55		

Note: The circumferential coordinate system is defined 0° = TDC, counter-clockwise, looking upstream

Note: The axial coordinate system is identified at the blade stacking line (X=1.21).

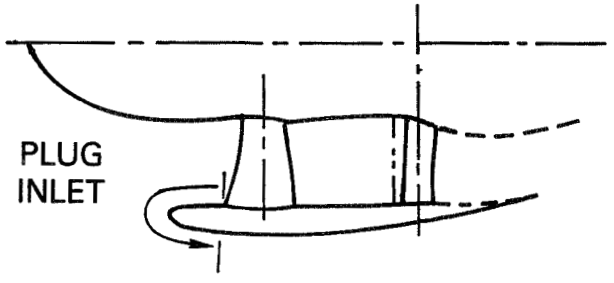

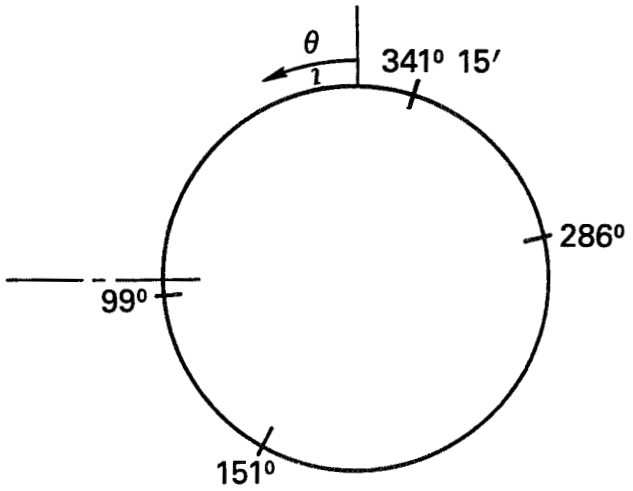

UTRC SETUP STATIC TAP ASSIGNMENTS AT FAN FACE POSITION 2

RAKE(I)	PSIDFF(I)	PSODFF(I)
A	1	1
B	5	5
C(POLE)	7	7
C(B.L.)	4	4
D	7	7
E	6	6
F	8	8
H	1	1

NASA SETUP STATIC TAP ASSIGNMENTS AT FAN FACE POSITION 2

RAKE(I)	PSIDFF(I)	PSODFF(I)
A	1	1
B	1	1
C(POLE)	7	7
C(B.L.)	4	4
D	7	7
E	6	6
F	8	8
H	2	2

UTRC SETUP

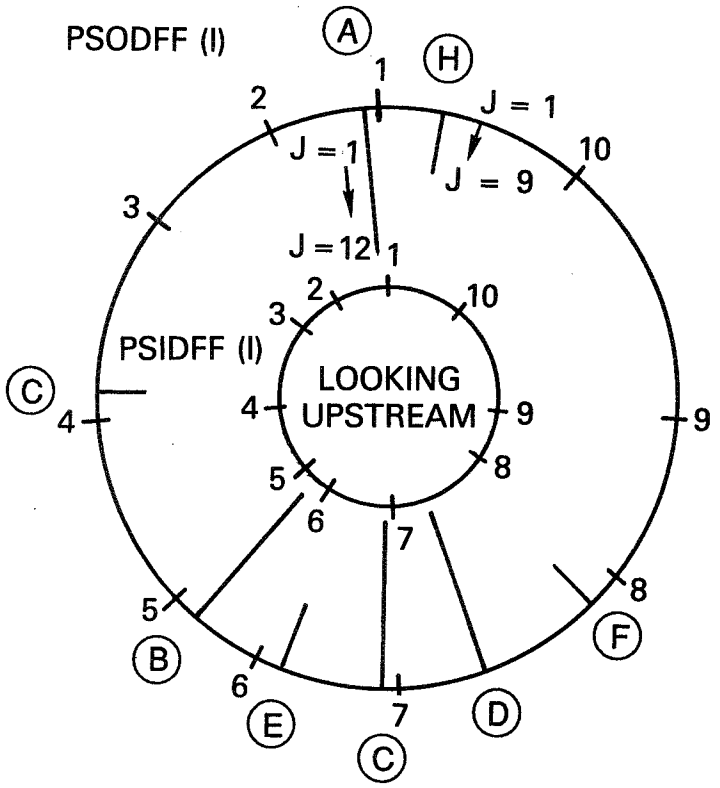

Fan Face Position 2

NASA LeRC SETUP

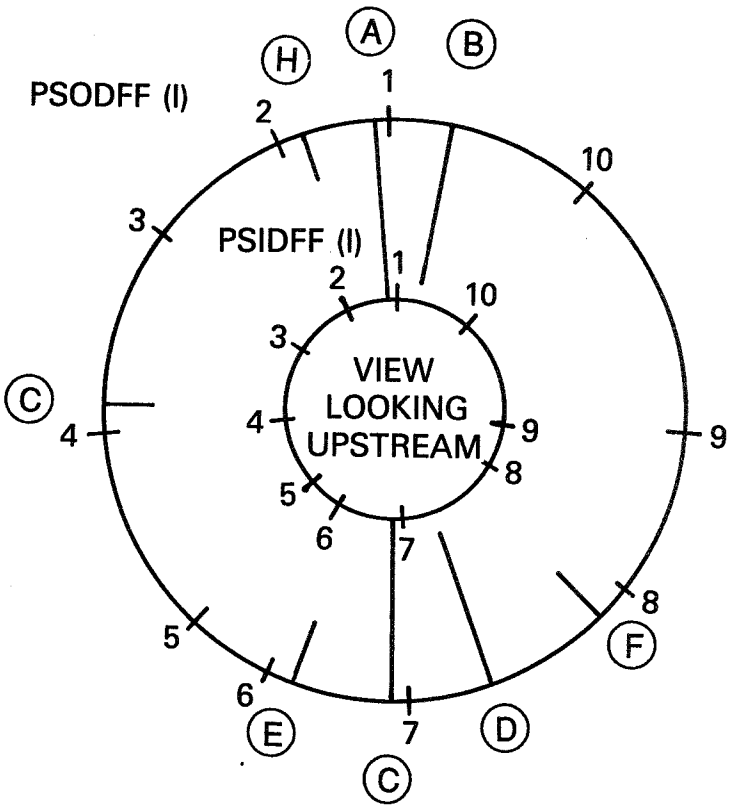

Fan Face Position 2

UTRC SETUP AREA BREAKUP AT POSITION 2 (FAN FACE)

RAKE	PROBE	AREA(I,J)	RADIUS(I,J)	% SPAN(I,J)	AREA FACTOR(I,J)
A	1	0.3657	8.379	0.9603	0.7314
POSITION	2	0.2417	8.153	0.9126	0.4834
5 DEG.	3	0.2355	7.926	0.8647	0.4710
	4	0.2283	7.699	0.8168	0.4566
	5	3.3170	7.473	0.7679	6.6340
	6	5.4828	7.246	0.7213	10.9656
	7	7.1163	6.793	0.6257	14.2326
	8	6.6488	6.340	0.5301	13.2976
	9	6.1732	5.886	0.4344	12.3464
	10	4.8675	5.433	0.3388	9.7350
	11	4.7841	5.116	0.2719	9.5682
	12	10.4501	4.617	0.1667	20.9002

RAKE	PROBE	AREA(I,J)	RADIUS(I,J)	% SPAN(I,J)	AREA FACTOR(I,J)
B	1	0.6094	8.379	0.9603	1.2188
POSITION	2	0.4029	8.153	0.9126	0.8058
140 DEG.	3	0.3925	7.926	0.8647	0.7850
	4	0.3805	7.699	0.8168	0.7610
	5	0.5087	7.473	0.7679	1.0174
	6	0.7241	7.246	0.7213	1.4482
	7	0.9399	6.793	0.6257	1.8798
	8	0.8781	6.340	0.5301	1.7562
	9	0.8153	5.886	0.4344	1.6306
	10	0.6429	5.433	0.3388	1.2858
	11	0.6319	5.116	0.2719	1.2638
	12	1.3802	4.617	0.1667	2.7604

RAKE	PROBE	AREA(I,J)	RADIUS(I,J)	% SPAN(I,J)	AREA FACTOR(I,J)
C(B.L.)	1	0.7561	8.556	0.9976	1.5122
POSITION	2	0.5516	8.516	0.9892	1.1032
90 DEG.	3	0.7310	8.466	0.9786	1.4620
	4	1.0267	8.396	0.9639	2.0534
	5	1.3725	8.296	0.9428	2.7450
	6	1.7034	8.166	0.9153	3.4068
	7	2.0724	8.006	0.8816	4.1448
	8	2.2480	7.806	0.8394	4.4960
	9	1.8275	7.606	0.7972	3.6550

RAKE	PROBE	AREA(I,J)	RADIUS(I,J)	% SPAN(I,J)	AREA FACTOR(I,J)
C(POLE)	1	0.9751	8.379	0.9603	1.9502
POSITION	2	0.6446	8.153	0.9126	1.2892
180 DEG	3	0.6280	7.926	0.8647	1.2560
	4	0.6087	7.699	0.8168	1.2174
	5	0.6165	7.473	0.7692	1.2330
	6	0.5485	7.246	0.7213	1.0970
	7	0.5550	7.019	0.6734	1.1100
	8	0.7983	6.793	0.6257	1.5966
	9	1.0036	6.340	0.5302	2.0072
	10	0.9318	5.886	0.4344	1.8636
	11	0.7347	5.433	0.3388	1.4694
	12	2.2995	5.116	0.2719	4.5990

RAKE	PROBE	AREA(I,J)	RADIUS(I,J)	% SPAN(I,J)	AREA FACTOR(I,J)
D	1	0.2486	8.379	0.9603	0.2486*
POSITION	2	0.4126	8.153	0.9126	0.4126*
200 DEG.	3	0.2763	7.926	0.8647	0.5526
	4	0.2689	7.699	0.8168	0.5378
	5	0.4937	7.473	0.7692	0.9874
	6	0.5485	7.246	0.7213	1.0970
	7	0.5550	7.019	0.6734	1.1100
	8	0.7983	6.793	0.6257	1.5966
	9	1.0036	6.340	0.5302	1.0072
	10	0.9318	5.886	0.4344	1.8636
	11	0.7347	5.433	0.3388	1.4694
	12	2.2995	5.116	0.2719	4.5990

RAKE	PROBE	AREA(I,J)	RADIUS(I,J)	% SPAN(I,J)	AREA FACTOR(I,J)
E	1	0.1833	8.556	0.9976	0.3666
POSITION	2	0.1337	8.516	0.9892	0,2674
160 DEG.	3	0.2022	8.466	0.9786	0.4044
	4	0.2486	8.396	0.9639	0.2486*
	5	0.3266	8.296	0.9428	0.6532
	6	0.4126	8.166	0.9153	0.4126*
	7	0.3179	8.006	0.8816	0.6358
	8	0.3095	7.806	0.8394	0.6190
	9	0.2996	7.606	0.7972	0.5992

RAKE	PROBE	AREA(I,J)	RADIUS(I,J)	% SPAN(I,J)	AREA FACTOR(I,J)
F	1	0.0458	8.556	0.9976	0.0916
POSITION	2	0.0334	8.516	0.9892	0.0668
225 DEG.	3	0.0443	8.466	0.9786	0.0886
	4	0.0622	8.396	0.9639	0.1244
	5	0.0832	8.296	0.9428	0.1664
	6	0.1032	8.166	0.9153	0.2064
	7	0.1256	8.006	0.8816	0.2512
	8	0.1362	7.806	0.8394	0.2724
	9	0.1108	7.606	0.7972	0.2216

RAKE	PROBE	AREA(I,J)	RADIUS(I,J)	% SPAN(I,J)	AREA FACTOR(I,J)
H	1	0.3895	8.556	0.9976	0.7790
POSITION	2	0.2842	8.516	0.9892	0.5684
350 DEG.	3	0.3766	8.466	0.9786	0.7532
	4	0.5289	8.396	0.9639	1.0578
	5	0.7070	8.296	0.9428	1.4140
	6	0.8775	8.166	0.9153	1.7550
	7	1.0676	8.006	0.8816	2.1352
	8	1.1580	7.806	0.8394	2.3160
	9	0.9414	7.606	0,7972	1.8828

NASA SETUP AREA BREAK-UP

RAKE	PROBE	AREA(I,J)	RADIUS(I,J)	% SPAN(I,J)	AREA FACTOR(I,J)
A	1	0.3657	8.379	0.9603	0.7314
POSITION	2	0.2417	8.153	0.9126	0.4834
5 DEG.	3	0.2355	7.926	0.8647	0.4710
	4	0.2283	7.699	0.8168	0.4566
	5	0.2312	7.473	0.7679	0.4624
	6	0.3103	7.246	0.7213	0.6206
	7	0.4028	6.793	0.6257	0.8056
	8	0.3763	6.340	0.5301	0.7526
	9	0.3494	5.886	0.4344	0.6988
	10	0.2755	5.433	0.3388	0.5510
	11	0.2708	5.116	0.2719	0.5416
	12	0.5915	4.617	0.1667	1.1830

RAKE	PROBE	AREA(I,J)	RADIUS(I,J)	% SPAN(I,J)	AREA FACTOR(I,J)
B	1	0.3657	8.379	0.9603	0.7314
POSITION	2	0.2417	8.153	0.9126	0.4834
350 DEG.	3	0.2355	7.926	0.8647	0.4710
	4	0.2283	7.699	0.8168	0.4566
	5	0.3546	7.473	0.7679	0.7092
	6	0.5172	7.246	0.7213	1.0344
	7	0.6713	6.793	0.6257	1.3426
	8	0.6272	6.340	0.5301	1.2544
	9	0.5824	5.886	0.4344	1.1648
	10	0.4592	5.433	0.3388	0.9184
	11	0.4513	5.116	0.2719	0.9026
	12	0.9859	4.617	0.1667	1.9718

RAKE	PROBE	AREA(I,J)	RADIUS(I,J)	% SPAN(I,J)	AREA FACTOR(I,J)
C(B.L.)	1	0.8020	8.556	0.9976	1.6040
POSITION	2	0.5851	8.516	0.9892	1.1702
90 DEG.	3	0.7753	8.466	0.9786	1.5506
	4	1.0889	8.396	0.9639	2.1778
	5	1.4557	8.296	0.9428	2.9114
	6	1.8066	8.166	0.9153	3.6132
	7	2.1980	8.006	0.8816	4.3960
	8	2.3842	7.806	0.8394	4.7684
	9	1.9383	7.606	0.7972	3.8766

RAKE	PROBE	AREA(I,J)	RADIUS(I,J)	% SPAN(I,J)	AREA FACTOR(I,J)
C(POLE)	1	0.9751	8.379	0.9603	1.9502
POSITION	2	0.6446	8.153	0.9126	1.2892
180 DEG.	3	0.6280	7.926	0.8647	1.2560
	4	0.6087	7.699	0.8168	1.2174
	5	0.6165	7.473	0.7692	1.2330
	6	0.5485	7.246	0.7213	1.0970
	7	0.5550	7.019	0.6734	1.1100
	8	0.7983	6.793	0.6257	1.5966
	9	1.0036	6.340	0.5302	2.0072
	10	0.9318	5.886	0.4344	1.8636
	11	0.7347	5.433	0.3388	1.4694
	12	2.2995	5.116	0.2719	4.5990

RAKE	PROBE	AREA(I,J)	RADIUS(I,J)	% SPAN(I,J)	AREA FACTOR(I,J)
D	1	0.2797	8.379	0.9603	0.2797*
POSITION	2	0.4642	8.153	0.9126	0.4642*
200 DEG.	3	0.3109	7.926	0.8647	0.6218
	4	0.3025	7.699	0.8168	0.6050
	5	3.7030	7.473	0.7692	7.4060
	6	4.1136	7.246	0.7213	8.2272
	7	4.1622	7.019	0.6734	8.3244
	8	5.9872	6.793	0.6257	11.9744
	9	7.5269	6.340	0.5302	15.0538
	10	6.9885	5.886	0.4344	13.9770
	11	5.5103	5.433	0.3388	11.0206
	12	17.2463	5.116	0.2719	34.4926

RAKE	PROBE	AREA(I,J)	RADIUS(I,J)	% SPAN(I,J)	AREA FACTOR(I,J)
E	1	0.2062	8.556	0.9976	0.4124
POSITION	2	0.1504	8.516	0.9892	0.3008
160 DEG.	3	0.2275	8.466	0.9786	0.4550
	4	0.2797	8.396	0.9639	0.2797*
	5	0.3675	8.296	0.9428	0.7350
	6	0.4642	8.166	0.9153	0.4642*
	7	0.3576	8.006	0.8816	0.7152
	8	0.3481	7.806	0.8394	0.6962
	9	0.3371	7.606	0.7972	0.6742

RAKE	PROBE	AREA(I,J)	RADIUS(I,J)	% SPAN(I,J)	AREA FACTOR(I,J)
F	1	0.3208	8.556	0.9976	0.6416
POSITON	2	0.2340	8.516	0.9892	0.4680
225 DEG.	3	0.3101	8.466	0.9786	0.6202
	4	0.4356	8.396	0.9639	0.8712
	5	0.5823	8.296	0.9428	1.1646
	6	0.7226	8.166	0.9153	1.4452
	7	0.8792	8.006	0.8816	1.7584
	8	0.9537	7.806	0.8394	1.9074
	9	0.7753	7.606	0.7972	1.5506

RAKE	PROBE	AREA(I,J)	RADIUS(I,J)	% SPAN(I,J)	AREA FACTOR(I,J)
H	1	0.0917	8.556	0.9976	0.1834
POSITION	2	0.0669	8.516	0.9892	0.1338
20 DEG.	3	0.0886	8.466	0.9786	0.1772
	4	0.1244	8.396	0.9639	0.2488
	5	0.1664	8.296	0.9428	0.3328
	6	0.2065	8.166	0.9153	0.4130
	7	0.2512	8.006	0.8816	0.5024
	8	0.2725	7.806	0.8394	0.5450
	9	0.2215	7.606	0.7972	0.4430

APPENDIX C

LIST OF SYMBOLS

LIST OF SYMBOLS

Test Conditions

AOA	Engine centerline angle of attack (degrees)
MO	Free stream Mach number
PSO	Free stream static pressure (psia)
PTO	Free stream total pressure (psia)
QO	Free stream dynamic pressure (psia)
RNO	Free stream Reynolds No./ft.
TTO	Free stream total temperature (R)
VOFPS	Free stream velocity (ft/sec)
VOKTS	Free stream velocity (knots)

Model Geometry

Aff	Area at fan face–plane of fan leading edge in 17" rig–square inches
Ahi	Highlight area–square inches
Dhi	Highlight diameter–inches
Dmax	Maximum nacelle diameter – inches
Dt	Inlet throat diameter – inches
Lin	Length of the inlet–inches
Lplug	Length of the plug – inches

Greek Letters

ϕR	Circumferential coverage of rods
ϕS	Circumferential coverage of screens
ϕO	Circumferential coverage of open area
θR	Location of rods blockage center
θS	Location of screen blockage center
θO	Location of open area center

Pressure Measurements and Coefficients

PTBL(i,j) Inlet boundary layer total pressure (psia)

PT(i,j) Inlet total pressures (psia)

PSAX(i,j) Inlet axial surface static pressures (psia)

PSFFI(i) Fan face circumferential static pressures on inner wall (psia)

PSFFO(i) Fan face circumferential static pressures on outer wall (psia)

PS10(i) Inlet surface static pressures on outer wall (psia)

CPAX(i,j) Pressure coefficient corresponding to PSAS(i,j)

PSRAKE(i,j) Local static pressure (psia)

MNRAKE(i,j) Local Mach number

MDOT(i,j) Local flow parameter

A(i,j) Area factor (in)

PTMAFF Mass averaged total pressure at fan face (psia)

PTAAFF Area averaged total pressure at fan face (psia)

P2AA Area averaged total pressure at inlet position 1 (psia)

Inlet Flow and Pressure Recovery

WFVEN Metered inlet air flow (lbs/sec)

WFCORR Metered inlet air flow corrected to standard day conditions using free stream conditions (lbs/sec)

WFNASA Inlet air flow corrected to standard day conditions using free stream conditions from analytical calibration (lbs/sec)

MFR Mass flow ratio using WFCORR

IDISTO Distortion Factor using free stream total pressure

IDIST1 Distortion Factor using area averaged total pressure at position 1

IDIST2 Distortion Factor using mass averaged total pressure at position 2

IRAM1 Area averaged total pressure recovery factor at position 1

IRAMA2 Area averaged total pressure recovery factor at fan face

IRAMM2 Mass averaged total pressure recovery factor at fan face

NASA
National Aeronautics and Space Administration

Report Documentation Page

1. Report No.	2. Government Accession No.	3. Recipient's Catalog No.
NASA CR–189149		

4. Title and Subtitle	5. Report Date
Ultra High bypass Nacelle Aerodynamics Inlet Flow–Through High Angle of Attack Distortion Test	July 1992
	6. Performing Organization Code
7. Author(s)	8. Performing Organization Report No.
Michael J. Larkin, Paul S. Schweiger	PWA–6354
	10. Work Unit No.
	535–03–10
9. Performance Organization Name and Address	11. Contract or Grant No.
UTC–Pratt & Whitney 400 Main Street East Hartford, Connecticut 06108	NAS3–25952
	13. Type of Report and Period Covered
12. Sponsoring Agency Name and Address	Final Report
NASA–Lewis Research Center 21000 Brookpark Road Cleveland, Ohio 44135	14. Sponsoring Agency Code

15. Supplementary Notes

Project Manager, Donald R. Boldman, Propulsion Systems Division, NASA Lewis Research Center, Cleveland, Ohio

16. Abstract

A flow–through inlet test program was conducted to evaluate inlet test methods and determine the impact of the fan on inlet separation when operating at large angles of attack. A total of 16 model configurations of approximately 1/6 scale were tested. A comparison of these flow–through results with powered data indicates the presence of the fan increased separation free operation 3° to 4° over the flow through inlet. Rods and screens located at the fan face station, that redistribute the flow, achieved simulation of the powered–fan results for separation angle of attack. Concepts to reduce inlet distortion and increase angle of attack capability were also evaluated. Vortex generators located on the inlet surface increased inlet angle of attack capability up to 2° and reduced inlet distortion in the separated region. Finally, a method of simulating the fan/inlet aerodynamic interaction using blockage sizing method has been defined. With this method, a static blockage device used with a flow–through model will approximate the same inlet onset of separation angle of attack and distortion pattern that would be obtained with an inlet model containing a powered fan.

17. Key Words (Suggested by Author(s))	18. Distribution Statement
Inlet Flow; Shrouded Propellers; Flow Distortion; Angle of Attack; Vortex Generators; Boundary Layer Control	Unclassified–Unlimited

19. Security Classif. (of this report)	20. Security Classif. (of this page)	21. No. of pages	22. Price
Unclassified	Unclassified	71	A04